

THEORY OF VACANCIES AND CORE EXCITONS
NEAR SEMICONDUCTOR SURFACES

Thesis by

Murray Scott Daw

In Partial Fulfillment of the Requirement
for the Degree of
Doctor of Philosophy

California Institute of Technology
Pasadena, California

1981

To my beloved wife
and parents

ACKNOWLEDGEMENTS

I would like to thank Professors Darryl L. Smith and Tom McGill for their assistance and enthusiasm during the course of this work. I also benefited from discussions and friendships with Dr. Yia-Chung Chang, Reuben Collins, Dr. Ken Elliott, Randy Feenstra, Prof. Bill Goddard, Andy Hunter, Dr. Ralph James, Dr. Tom Kuech, Christian Mailhiot, Gordon Mitchard, Dr. Gordon Osbourn, Arati Prabhakar, Dr. J. N. Schulman, Dr. Coenraad Swarts, Mike Weimer, and Amikam Zur. Thanks go to Dr. Swarts for allowing me to use one of his figures. I would like to express my gratitude to Vere Snell for typing this thesis and for her cheerful smile and excellent secretarial help.

I am thankful for financial support from the California Institute of Technology, the ARCS Foundation, and the Office of Naval Research.

Most importantly, I thank my wife, Lili, and my parents for their encouragement and support during my student years and for their assistance with the manuscript and figures.

ABSTRACT

This thesis presents theoretical treatments of vacancies and core excitons on semiconductor surfaces. After an introduction to the subject, the general Koster-Slater approach in the tight-binding approximation is reviewed. Realistic tight-binding parameters for a number of III-V and II-VI semiconductors are obtained. Chapter 3 then deals with semiconductor surface core excitons. Vacancies near a semiconductor surface are treated in Chapter 4.

We present in the third chapter calculations of the binding energies and oscillator strengths of surface core excitons. Results for the (110) surface of GaAs, GaP, GaSb, and InP are included. We find that transitions from core levels to the surface dangling bonds allow the confinement of the electron to the region near the hole, producing a Frenkel exciton. We find that transitions out of the cation d core to the large p component of the dangling bond lead to observable excitons. Transitions from the cation p core couple to the small s component of the surface state and have similar binding but damped oscillator strength. It is found that transitions from the anion core should produce no exciton.

In the fourth chapter, we show calculations of the bound state levels of vacancies near semiconductor surfaces. We present results

for ideal vacancy levels in bulk and near the (110) surface of GaSb, GaAs, GaP, InAs, AlAs, InP, ZnTe, CdTe, ZnSe, $\text{Ga}_x\text{In}_{1-x}\text{As}$, $\text{Ga}_x\text{Al}_{1-x}\text{As}$, and $\text{Ga}_x\text{In}_{1-x}\text{P}$. We find that ideal vacancy levels are changed by less than 0.1 eV as the vacancy is moved near the surface until it reaches the second layer from the surface. On the surface, the highest occupied level in the neutral anion vacancy goes to higher energy and that in the cation vacancy goes to lower energy.

General trends are noted for comparisons between covalent and more ionic materials. Cation vacancy levels tend to move toward the valence band and anion levels toward the conduction band as one considers increasingly ionic compounds. We consider also the Jahn-Teller effect (lattice distortion) and Coulomb repulsion among the bound electrons. These effects cause the various charge states of vacancies to have different energies. Vacancies in III-V's and II-VI's show qualitatively different behavior. A neutral vacancy in a III-V compound has an odd number of electrons and so can have both donor and acceptor roles. A neutral vacancy in a II-VI semiconductor has an even number and takes on either double acceptor or double donor character, depending on the specifics.

The Defect Model of Schottky barrier formation is also investigated in Chapter 4, and it is concluded that anion vacancies in III-V semiconductors can account for the observed properties of Fermi level pinning. The role of vacancies in pinning the Fermi level of II-VI materials is uncertain.

Parts of this thesis have been or will be published under the following titles:

Chapter 3:

"Summary Abstract: Surface Core Excitons in III-V Semiconductors", M. S. Daw, D. L. Smith, and T. C. McGill, J. Vac. Sci. Technol. (to be published).

"III-V Semiconductor Surface Core Excitons", M. S. Daw, D. L. Smith, and T. C. McGill (in preparation).

Chapter 4:

"Vacancies Near Semiconductor Surfaces", M. S. Daw and D. L. Smith, Phys. Rev. B20, 5150 (1979).

"Surface Vacancies in InP and GaAlAs", M. S. Daw and D. L. Smith, Appl. Phys. Lett. 36, 690 (1980).

"Energy Levels of Semiconductor Surface Vacancies", M. S. Daw and D. L. Smith, J. Vac. Sci. Technol. 17, 1028 (1980).

"Relation Between the Common Anion Rule and the Defect Model of Schottky Barrier Formation", Solid State Commun, 37, 205 (1981).

"Surface Vacancies in II-VI and III-V Zinc Blende Semiconductor", J. Vac. Sci. Technol. (to be published).

A publication not included in this thesis is:

"Fano Resonance in Semiconductor Surface Core Excitons",
M. S. Daw, D. L. Smith, and T. C. McGill (in preparation).

TABLE OF CONTENTS

CHAPTER 1. INTRODUCTION	1
I. BACKGROUND	2
A. Surface Core Excitons	4
B. Schottky Barriers and Vacancies	6
II. OUTLINE OF THESIS	9
III. A PRIMER ON THE (110) GaAs SURFACE AND ON ULTRAVIOLET PHOTOEMISSION SPECTROSCOPY	10
REFERENCES	26
CHAPTER 2. BULK AND SURFACE BAND STRUCTURE CALCULATIONS	28
I. INTRODUCTION	29
II. THE TIGHT-BINDING HAMILTONIAN	31
III. GREEN'S FUNCTION IN SEMICONDUCTORS	43
IV. SUMMARY	58
REFERENCES	59
CHAPTER 3. SURFACE CORE EXCITONS IN SEMICONDUCTORS	61
I. INTRODUCTION	62
II. CALCULATION OF BINDING ENERGIES AND OSCILLATOR STRENGTHS	64
III. SUMMARY	75

REFERENCES	76
CHAPTER 4. VACANCIES NEAR SEMICONDUCTOR SURFACES	78
I. INTRODUCTION	79
II. IDEAL BULK VACANCIES	81
III. CHARGED VACANCY STATES AND THE JAHN-TELLER EFFECT	94
IV. IDEAL VACANCIES NEAR THE SURFACE	110
V. VACANCIES AND SCHOTTKY BARRIERS	121
VI. SUMMARY	137
APPENDIX	138
REFERENCES	143

CHAPTER 1
INTRODUCTION

I. BACKGROUND

The study of semiconductor surfaces has made great progress in the past decade. Surface-sensitive experiments, combined with theoretical analyses, are now capable of determining atomic geometries at the surface and can probe the electronic structure over a wide range of energies and with good resolution. Further progress is being made in the study of surface adsorption and the stages leading to interface and oxide formation.

Such advances are technologically important. In some electrical devices, interfaces between a metal and a semiconductor control the active regions where essential electronic functions occur. As miniaturization of these devices continues, surface and interface effects become more crucial. Control of the effects is highly desirable and may be vital to future development in the field, but in some ways remains beyond our present abilities. Consequently, there has been much interest in studying the fundamentals of interfaces and their formation. Several achievements have made these studies possible. The achievement of atomically clean semiconductor surfaces, prepared in ultra-high vacuum, has allowed the examination of the intrinsic states and surface structure. Low energy electron diffraction (LEED) techniques for structural analysis and ultraviolet photoemission spectroscopy (UPS) for probing the electronic con-

figurations have opened up great avenues of investigations. Controlled contamination studies yield further information on the chemistry and physics of interfaces. Theorists have contributed interpretations of complex data and investigations of proposals that would be difficult to test experimentally.

Such advances also are scientifically important. The termination of a crystal by the surface creates states that have no analog among the usual bulk phenomena. The surface-related states in many ways behave as localized entities neighboring the bulk crystal. When treated as though they were localized, they provide an interesting contrast to the more conventional solid state effects.

This thesis covers work in two areas of semiconductor surface physics: one, the theoretical treatment of core excitons on (110) III-V compounds; the other, the theory of the electronic states of vacancies close to the (110) surface of III-V and II-VI semiconductors. Both areas involve the theory of electronic states near the surface.

In connection with the first, the thesis presents a theoretical understanding of the large binding energies relative to the conduction band which have been reported for ultraviolet transitions from core levels to empty surface states. Some experiments have concluded that the exciton is bound by as much as 1 eV or more, ⁽¹⁾ compared to bulk core exciton binding energies of near 0.1 eV ⁽²⁾.

We also explore the possible connection between surface vacancies and Schottky barriers, and show that anion vacancies may indeed determine Schottky barrier heights in III-V semiconductors. This finding is consistent with evidence which has been presented on the effects of surface defects ⁽³⁾.

A. Surface Core Excitons

For nearly six years, investigators have known of tightly bound surface state core excitons in (110) GaAs ⁽⁴⁾. Photoemission experiments have shown the existence of these excitons in GaSb, GaP, and InP as well. The measurements of binding energies vary somewhat for the same material, but the values are all in the range of 0.1 to 1.5 eV ⁽⁵⁾. Excitons involving some core levels are prominent. Others have not been observed. For example, the transition from the Ga(3d) core to an empty surface state on (110) GaAs has been observed to produce an exciton, while that from Ga(3p) does not.

Despite the availability of data and an interest in a realistic theoretical description of surface core excitons, the theory has remained underdeveloped. Del Sole and Tosatti ⁽⁶⁾ calculated binding energies and wave functions of surface state excitons in semiconductors for a logarithmic potential. But their approach, based on the effective mass approximation, is invalid for surface

states and is therefore internally inconsistent. Altarelli, Bachelet, and Del Sole ⁽⁷⁾ developed an exactly soluble model of surface core excitons which involves a one-band description of a semiconductor. Their interaction potential is overly simplified and its form and the weak binding in bulk creates inconsistencies in their calculation. Wang and Joannopoulos ⁽⁸⁾ provided what was by far the best treatment at the time, with their calculation of the binding energy of Ga(3d) surface core excitons in (110) GaAs. However, their potential energy was also unrealistic and, even more seriously, they failed to allow for realistic surface geometry. The latter flaw makes their calculation unreliable, since it has been shown that surface electronic states are sensitive to atomic configuration. ⁽¹⁸⁾

The surface core exciton calculation presented in this thesis takes account of the factors not provided for in the theories just mentioned. Accurate surface geometries, realistic band structures, and reasonable potential are all included. Our calculation thus makes possible a unified treatment of excitons on a variety of materials from different possible core levels and reveals strong binding for certain excitons on the (110) surface of GaAs, GaP, and InP ⁽⁹⁾. The results are in good agreement with the available data. Key experiments are suggested to test our understanding of the effect.

B. Schottky Barriers and Vacancies

Schottky barriers have been made for many years but an explanation of what determines the barrier height has been elusive. A Schottky barrier is formed at the interface of a metal and a semiconductor. The Fermi level of the semiconductor is usually fixed by impurities and is generally different from that of the metal. When the two materials are brought into contact, electron transfer occurs to bring the Fermi level constant throughout the system. The charge transfer causes ionization of impurities near the interface in what is called the depletion region. This separation of charges causes the bands to bend near the interface, acting as a barrier to current.

Four empirical rules have been noted for these contacts (10). These are not fixed, but indicate trends:

(1) For some difference ΔX_M in the electronegativities of two metals, the barriers formed by the two metals on the same semiconductor differ by $S \cdot \Delta X_M$. Values for S range from near 0 to 1.0. Barriers with small S are said to be pinned, or to have a pinned Fermi level.

(2) If the semiconductors are ordered by some measure of their covalency, it becomes apparent that covalent materials are pinned, that is, have $S < 0.4$, while ionic semiconductors are less so, with $S \approx 1.0$.

(3) With few exceptions, the electron barriers on the covalent semiconductors are approximately two-thirds of the band gap.

(4) For two covalent semiconductors with the same anion, the hole barriers on Au will be similar. This common anion rule does not hold for semiconductors containing Al.

To these empirical rules of Schottky barrier heights, one can now add the fact, shown by Huijser and Van Laar ⁽¹¹⁾, that an atomically clean semiconductor surface usually is not pinned, that is, there is no band bending. Small coverages with metal or oxygen causes ⁽¹⁴⁾ bending. The development of the bending can be followed carefully and ~15% coverage appears to complete the change.

Possible explanations of the origin of the pinning have been advanced since at least 1947, when Bardeen ⁽¹²⁾ suggested that it might be due to the presence of surface states in the gap. Heine ⁽¹³⁾ offered a modification, pointing out that in a metal-semiconductor interface the semiconductor surface states will (11) extend throughout the metal. The experiments of Huijser and Van Laar, ⁽¹⁴⁾ and others, made it clear that these surface states in the band gap are not native to perfect, clean III-V surfaces, but are induced by the adsorption of any of several elements. Some effort has concentrated on analyzing the interaction of the dangling bond states with the metal. Conceivably, dangling bond resonances could occur in the gap in a metal-semiconductor interface ⁽¹³⁾, but this mechanism

cannot account for band bending of surfaces with less than a monolayer of metal atoms.

Spicer and co-workers ⁽¹⁴⁾ recently suggested that defects at the interface could cause states in the gap. Following that suggestion, calculations were begun to determine the energy levels of anion and cation vacancies near the surface ⁽¹⁵⁾. A description of this research is presented in this thesis. We here conclude that anion vacancies in III-V semiconductors may be responsible for the Fermi level pinning.

II. OUTLINE OF THESIS

The balance of this thesis is organized into three chapters.

Chapter 2 deals with the basic theoretical tools. The tight-binding method for bulk and surface band structure calculations is sketched. The Green's function method for calculating states due to imperfections in the crystal is then discussed.

In the third chapter, we present our work on surface core excitons. We compute binding energies and oscillator strengths of anion and cation, p- and d-core excitons on (110) GaSb, GaAs, GaP, and InP.

The last chapter represents a detailed investigation of anion and cation vacancy states near the (110) surface of GaSb, GaAs, GaP, InAs, AlAs, InP, ZnTe, CdTe, and ZnSe. Ideal vacancy states are calculated for vacancies in the bulk and near the surface. The Jahn-Teller effect is taken into account and applied to the various charge states of vacancies. Finally, we discuss the possible relationship between vacancies and Fermi level pinning and Schottky barriers.

III. A PRIMER ON THE (110) GaAs SURFACE AND ON ULTRAVIOLET PHOTOEMISSION SPECTROSCOPY

The investigation of the (110) surface of GaAs has been among the most successful studies of zinc blende surfaces. Ultraviolet photoemission spectroscopy (UPS)⁽¹⁹⁾ has been a major experimental tool. It may be in order at this point to provide some background on GaAs and the UPS technique.

The current and well-accepted model of the (110) GaAs surface structure is shown in Fig. (I.1)⁽¹⁶⁾. This geometry was determined by low energy electron diffraction (LEED)⁽¹⁷⁾. The surface atoms have relaxed from their bulk-terminated positions. The relaxation of the second and third layers is smaller. The distortions change the bond lengths by less than 3%. Each surface Ga and As atom is bonded to two surface neighbors and one neighbor on the second layer. The fourth bond of the usual bulk tetrahedral arrangement has been chopped off by the surface and each atom therefore has a dangling bond sticking out from the solid. The As dangling bond is fully occupied (with what is called a "lone pair") and the Ga dangling bond is empty. The bonds are hybrids of valence s and p states. Because of the direction of relaxation, the As atom moves out from the surface, giving its sp^3 dangling bond more s-character. The Ga atom sinks into the surface and makes its bonds with neighboring As atoms almost planar (sp^2), so that its dangling bond is largely p-like.

Figure 1.1. The (110) surface of GaAs. (a) Top view; (b) side view of projection in the $(\bar{1}\bar{1}0)$ plane after relaxation. Δz and ω are used to characterize the relaxation. From Ref. (16).

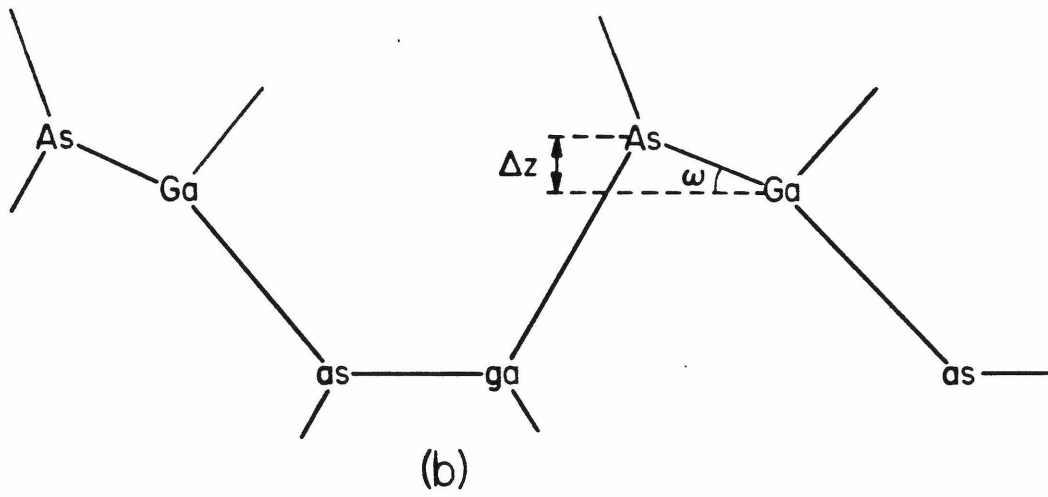
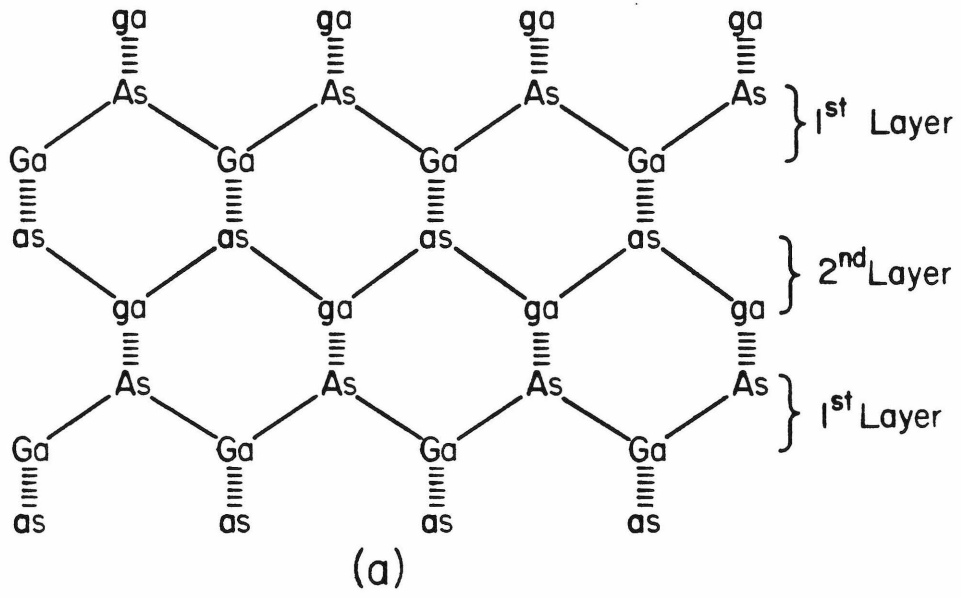


Figure 1.1

The electronic band structure of this kind of surface is shown schematically in Fig. (1,2). The usual valence and conduction band states are present, modified by the surface. In addition the dangling bonds introduce rather localized states resonant with the bulk bands. The filled As dangling bond is resonant with the valence band and the empty Ga dangling bond with the conduction band. If one were to perform calculations of the bands at the surface without allowing for the relaxation pictured in Fig. (1.1), the dangling bond states would generally be in the fundamental band gap.⁽¹⁸⁾ The surface relaxation pushes the dangling bond states into the bands (the As dangling bond takes on more s-character and its energy decreases, while the energy of the Ga dangling bond becomes more p-like and goes up). It is thus important in electronic structure calculations of the surface to include the relaxation.

The use of UV photoemission as a spectroscopic tool was pioneered in the 1950s and brought to a well-developed stage by the 1970s.⁽¹⁹⁾ The objective of UPS is to determine the energy distribution of electrons excited by monochromatic radiation and to deduce from this information about the electronic structure of the solid. The surface sensitivity of UPS (in the photon energy range of 15 to 100 eV or more) is determined by the escape depth, which is typically around 5 to 20 Å for these experiments. Some tuning of the depth can be obtained by varying the incident photon energy,

Figure 1.2. Schematic of the band structure of the (110) GaAs surface.

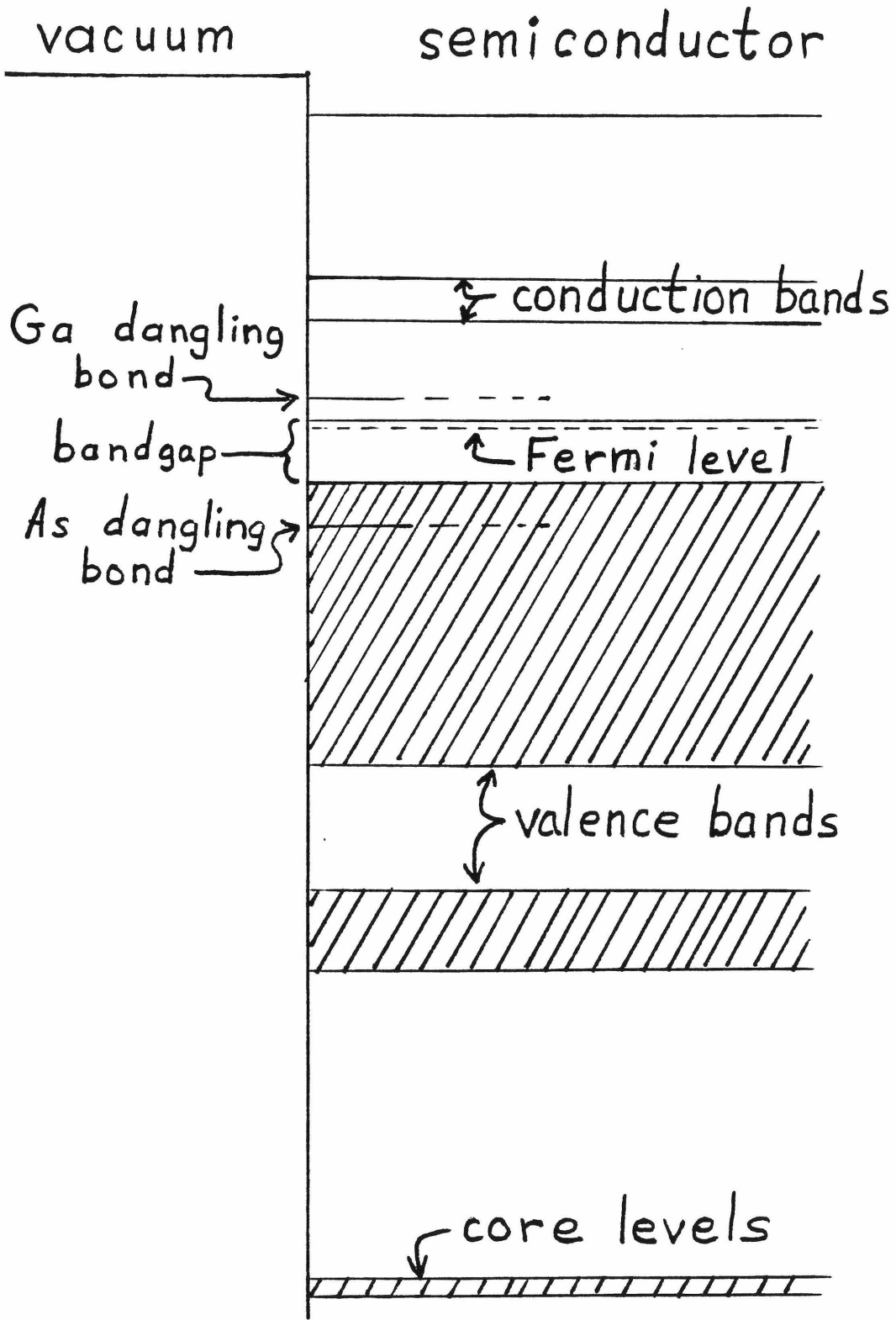


Figure 1.2

Figure (1,3) is a schematic diagram of the photoemission process. Electrons from the occupied states are excited by photons of energy $h\nu$ into the conduction band and make their way into the vacuum. Electron-electron scattering slows many of the excited electrons and produces a broad background of secondaries. The low-energy tail of the distribution is cut off by the potential barrier at the surface, while the higher energy electrons pass into the vacuum where their spectrum can be analyzed. In Figure (1.4), we see that some of the current is due to electrons excited directly from the valence bands. Other electrons are from an Auger process, where a core electron is excited to a relatively low-lying conduction band, a valence electron then falls into the core hole and a second valence electron is promoted to high energy. Still others are from a direct recombination process, in which the excited core electron recombines with its own hole and kicks a valence electron to the same energy it would possess if it were excited directly. In the last two processes, the emitted current can be enhanced by a resonant transition from the core to some unoccupied level.

The resulting spectrum for fixed $h\nu$ is called an energy distribution curve (EDC). Much of the band structure information can be deduced from the EDC's. For $h\nu \geq 25$ eV, the EDC gives a reasonable replica of the valence band density of states. Two other spectral techniques are commonly practiced in UPS: con-

Figure 1.3. Schematic of the photoemission process, visualized in three steps: excitation, transport, and escape. E_g is the fundamental band gap, $h\nu$ is the photon energy, and E_0 is the barrier to vacuum. See Ref. 19.

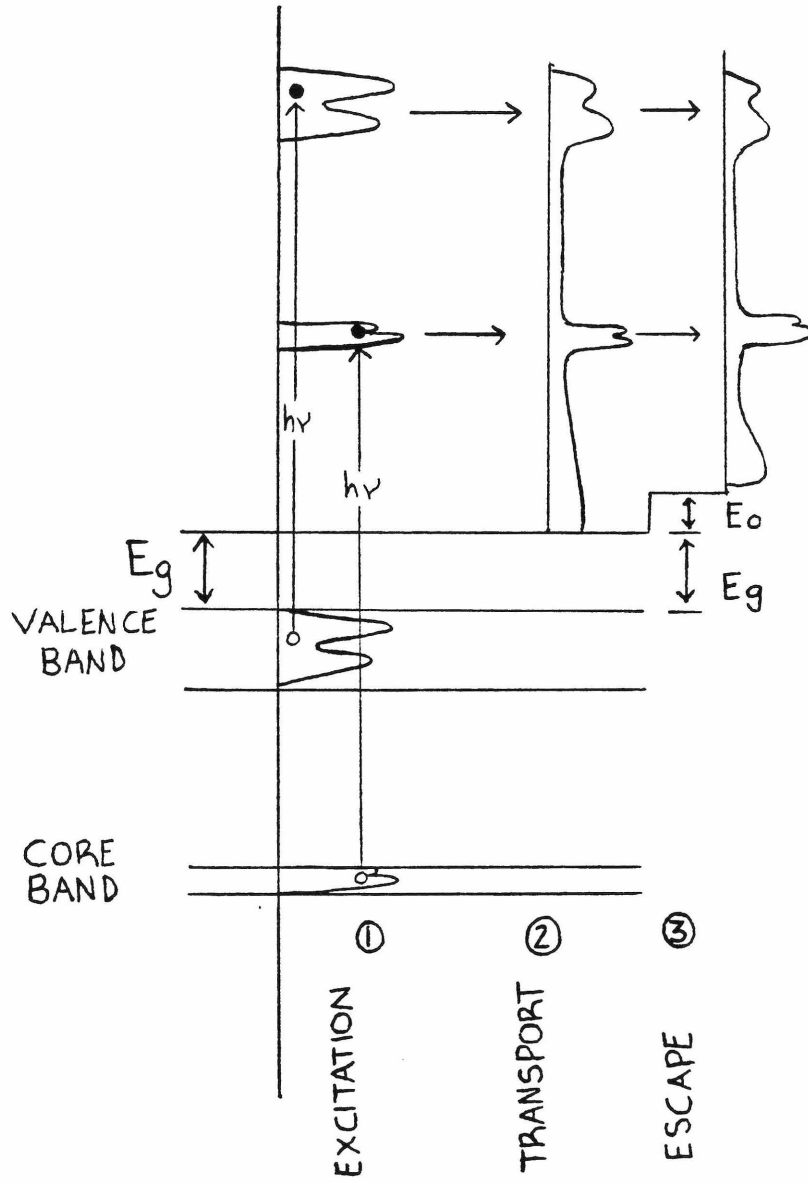


Figure 1,3

Figure 1.4. Three absorption processes contributing to electrons in the conduction band: direct excitation, Auger excitation, and direct recombination excitation. The photon energy is $h\nu$, the fundamental band gap is E_g , and E_o is the barrier to the vacuum.

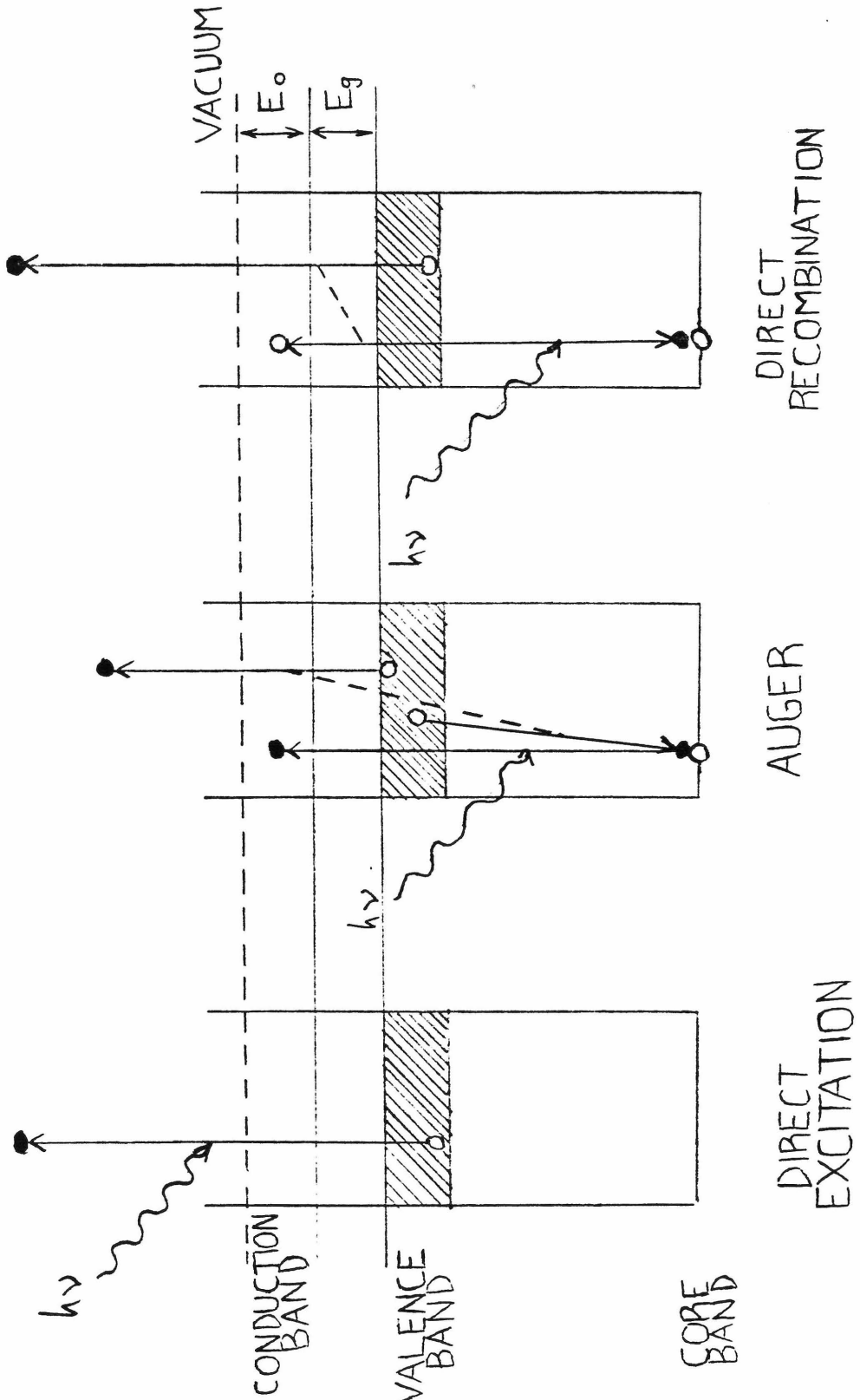


Figure 1.4

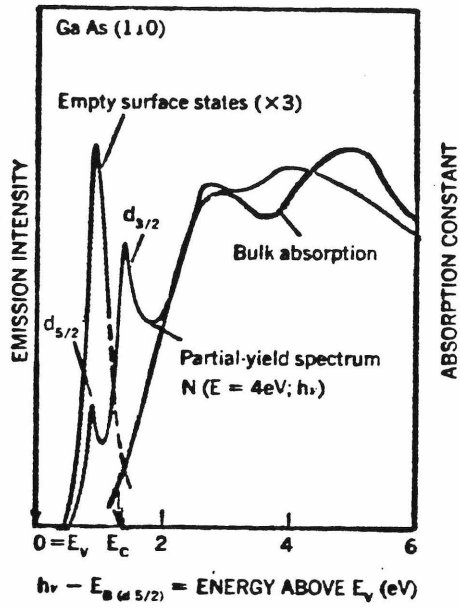
stant final state (CFS) and constant initial state (CIS)⁽²⁰⁾. A CFS spectrum (also called a partial yield spectrum) is obtained by fixing the electron analyzer to register only electrons at some fixed energy E_f above the valence band maximum, and then varying $h\nu$. A CIS spectrum is obtained by shifting E_f along with $h\nu$ so that $-E_i = h\nu - E_f$ is fixed. The use of one technique or the other allows identification of various features in the spectra depending on their origin, as will be seen in the following. The UPS technique can be used to locate band structure features relative to the Fermi level (fixed by a metal contact on the back of the sample), and in particular those features related to the surface.

Surface states related to the Ga dangling bond were first reported in 1975 by D. E. Eastman and J. L. Freeouf using CFS for (110) GaAs.⁽²¹⁾ The spectrum (see Fig. (1.5a)) showed two peaks related to transitions from the spin-orbit split core levels to the Ga dangling bond. These peaks appear in the band gap and can be eliminated by slight overlayers that tie up the dangling bonds. Eastman and Freeouf concluded that the peaks in the spectrum were at the dangling bond energies, placing them in the gap.

This interpretation of the CFS peaks agreed with Bardeen's 1947 theory.⁽¹²⁾ Bardeen had suggested that the dangling bond states were responsible for Fermi level pinning in semiconductors (see Fig. (1.5b)). At the time, there was no way to test Bardeen's

Figure 1.5. (a) Partial-yield (or CFS) spectrum for Ga(3d) transitions in (110) GaAs, from Ref. 21. (b) Surface band structure as interpreted by authors of Ref, 21.

a)



b)

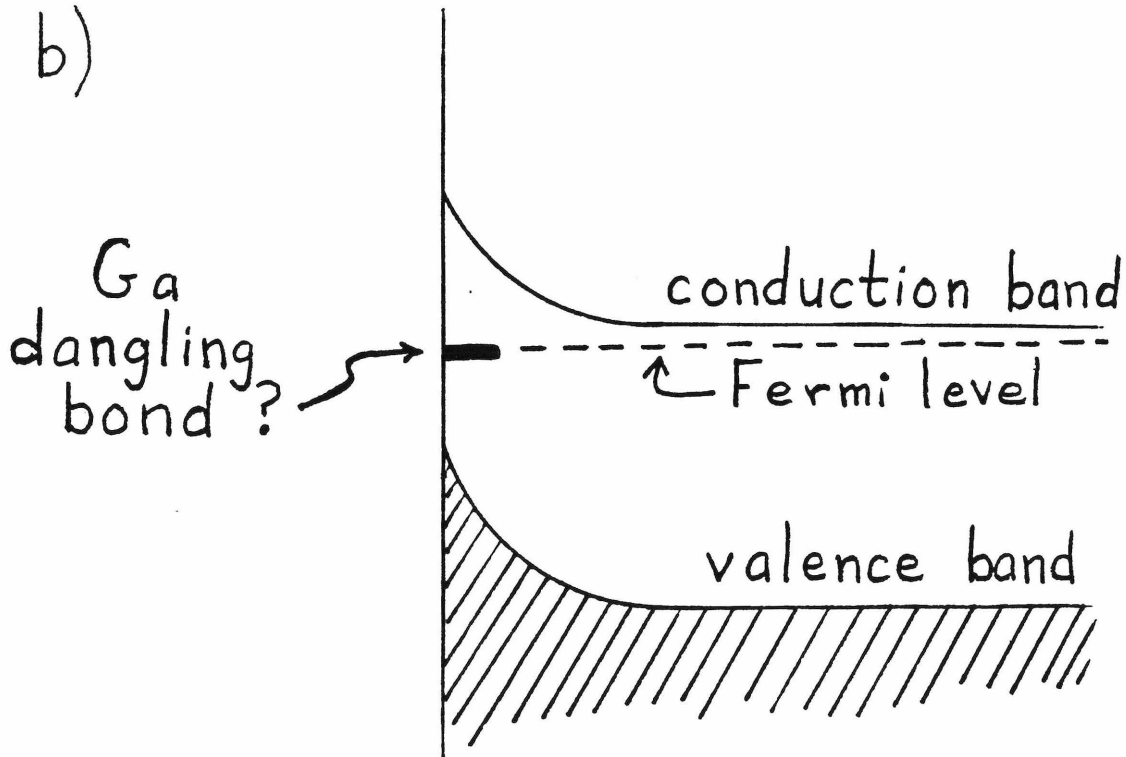


Figure 1.5

proposal on a free surface, but metal contacts could be formed and the band bending then shows up as the Schottky barrier. It was known that the Schottky barrier height (related to the degree of band bending) did not depend strongly on the work function of the metal used, and consequently the Fermi level must be pinned. Bardeen proposed a density of states in the gap, created by the dangling bonds, that served to restrict the Fermi level to a narrow range.

Huijser and Van Laar changed the interpretation with evidence that no band gap states were present in (110) GaAs.⁽¹¹⁾ Gudat and Eastman⁽²²⁾ supported this with UPS measurements of the degree of band bending of well-cleaved crystals in ultra-high vacuum. No band-bending occurred on a perfect, clean surface.

(14)

Spicer and co-workers confirmed that no band gap states exist on (110) GaAs (i.e., Fig. (1.2) is the case) and that as little as 1/100th of a monolayer of adatom caused significant bending. The asymptotic value of the bending (i.e., after 15% of a monolayer) was independent of adatom over a wide range of electronegativity (including Cs, Al, Ga, In, Au, and O adatoms). The band bending was also somewhat influenced by doping, being 0.3 eV or so different for n- and p-type GaAs.

The rather insensitive nature of the pinning on GaAs to adatom is reminiscent of the metal-independent Schottky barrier heights

on the same material. Yet it is clear that intrinsic surface states do not exist in the gap. A natural conclusion might be that the adsorption of metals or oxygen could cause defects in the lattice structure. ⁽¹⁴⁾ These defects may produce band gap states and pin the Fermi level. Indeed, imperfectly cleaved crystals, even though clean, were pinned, presumably by defects.

So now we may have some idea of what is causing the pinning. But what about the states seen clearly in Fig. (1.5a)? It was shown by Lapeyre and Anderson ⁽²³⁾ that these peaks were indeed due to transitions from the core to the Ga dangling bond, but that strong attraction between hole and electron produces a bound state which appears in the gap in a CFS spectrum, that is, an exciton.

REFERENCES

1. See references listed in Chapter 3.
2. D. E. Aspnes, C. G. Olson, and D. W. Lynch, *Phys. Rev.* B12, 2527 (1975). M. Altarelli, *Journ. de Phys.* C4, 95 (1978).
3. See references listed in Chapter 4.
4. G. J. Lapeyre and J. Anderson, *Phys. Rev. Lett.* 35, 117 (1975).
5. See Table 3.1.
6. R. Del Sole and E. Tosatti, *Solid State Commun.* 22, 307 (1977).
7. M. Altarelli, G. Bachelet, and R. Del Sole, *J. Vac. Sci. Technol.* 16, 1370 (1979).
8. Y. Wang and J. D. Joannopoulos, *J. Vac. Sci. Technol.* 17, 997 (1980).
9. M. S. Daw, D. L. Smith, and T. C. McGill, *J. Vac. Sci. Technol.* (to be published).
10. T. C. McGill and C. A. Mead, *J. Vac. Sci. Technol.* 11, 122 (1974). J. O. McCaldin, T. C. McGill, and C. A. Mead, *Phys. Rev. Lett.* 36, 56 (1976).
11. A. Huijser and J. Van Laar, *Surf. Sci.* 52, 202 (1975).
12. J. Bardeen, *Phys. Rev.* 71, 717 (1947).
13. V. Heine, *Phys. Rev.* 138, A1689 (1965), E. J. Mele and J. D.

- Joannopoulos, Phys. Rev. B17, 1528 (1978).
14. I. Lindau, P. W. Chye, C. M. Garner, P. Pianetta, C. Y. Su, and W. E. Spicer, J. Vac. Sci. Technol. 15, 1332 (1978).
P. W. Chye, I. Lindau, P. Pianetta, C. M. Garner, C. Y. Su, and W. E. Spicer, Phys. Rev. B18, 5545 (1978). W. E. Spicer, I. Lindau, P. Skeath, and C. Y. Su, J. Vac. Sci. Technol. 17, 1019 (1980).
 15. M. S. Daw and D. L. Smith, Phys. Rev. B20, 5150 (1979).
 16. C. W. Swarts, W. A. Goddard, and T. C. McGill, J. Vac. Sci. Technol. 17, 982 (1980).
 17. A. Kahn, E. So, P. Mark, C. B. Duke, R. J. Meyer, J. Vac. Sci. Technol. 15, 1223 (1978).
 18. E. J. Mele and J. D. Joannopoulos, Phys. Rev. 17, 1816 (1978).
See also Ref. 15.
 19. W. E. Spicer, Journ. de Phys. C6, 19 (1973). D. E. Eastman and M. I. Nathan, Physics Today, 28 #4, 44 (1975).
 20. G. J. Lapeyre, R. J. Smith, J. Knapp, and J. Anderson, Journ. de Phys. C4, 134 (1978).
 21. D. E. Eastman and J. L. Freeouf, Phys. Rev. Lett. 33, 1601 (1974).
 22. W. Gudat and D. E. Eastman, J. Vac. Sci. Technol. 13, 831 (1976).
 23. G. J. Lapeyre and J. Anderson, Phys. Rev. Lett. 35, 117 (1975).

CHAPTER 2

BULK AND SURFACE BAND STRUCTURE CALCULATIONS

I. INTRODUCTION

This chapter presents a method of calculating the band structure of a semiconductor in bulk or near the surface. With this information one can calculate the states resulting from defects or excitations in the material. In particular, we are interested in the deep levels which might be caused by a vacancy (atom missing from a lattice site) or core excitations formed from ultraviolet absorption by the semiconductor. The nature of these states is determined as much by the host as by the excitation or defect. Therefore, we first describe the states of the perfect semiconductor. Following that, we describe the method used to obtain the states of the imperfect or excited material.

There are several methods for computing band structures in semiconductors ⁽¹⁾. These vary in degree of rigor. For our purposes, we needed a method which would provide a realistic description of the bands within a few electron-volts on either side of the fundamental band gap and yet enable us to calculate states near the surface. We also wanted to develop descriptions of several semiconductors to compare the behavior between hosts. In addition, there are the usual limitations of the computer. A method such as the pseudopotential ⁽²⁾ or a variation of it, while it may be realistic, is slow and cumbersome. Calculating the surface states ⁽³⁾ is difficult enough for such a technique; to add a vacancy near the surface is impractical.

The tight-binding method ⁽⁴⁾ can be used for rapid calculations of bulk or surface band structures. The problem of handling a variety of materials reduces to fitting a non-linear function of 20 or so parameters for each required material. We therefore chose to use the tight-binding method discussed in the next section.

Once the description of the host semiconductor has been obtained, the electronic states of defects or excitations may be calculated. The theory of shallow states involving wave functions with characteristic lengths of 100 \AA or more has been successfully developed ⁽⁵⁾. For vacancies or excitations near the surface, states localized to the region of a few atoms may be produced. Such deep states have been treated with somewhat less success, depending more strongly on the local environment of the center than on the larger scale properties ⁽⁵⁾. For the deep states it becomes practical to use a Green's function method with a basis in position-space. This is described in the third section of this chapter.

With tight-binding Hamiltonian and the Green's function technique in hand, one may proceed to calculate in a practical fashion vacancy and core exciton states near the surface of a variety of semiconductors.

II. THE TIGHT-BINDING HAMILTONIAN

We would like to find a parametric approximation to the Hamiltonian such as the semi-empirical pseudopotential one ⁽²⁾ that produced the band structure shown in Fig. (2.1a). Such an approximate Hamiltonian could serve as a basis for calculations in cases in which the more sophisticated techniques, such as the one used for the figure, are very costly.

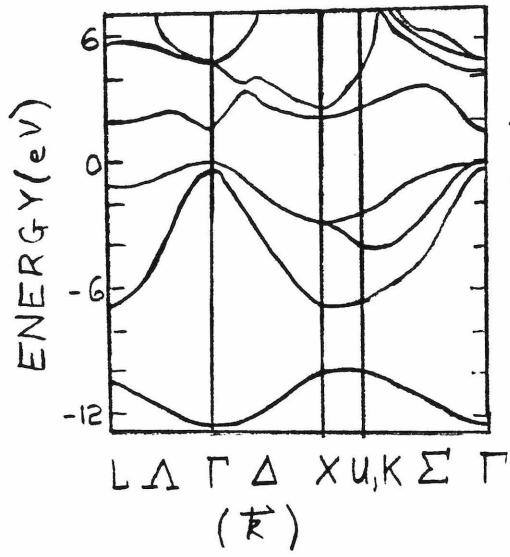
A natural form for such a Hamiltonian is suggested by the tight-binding theory. Here one begins by expressing a Bloch wave as a linear combination of localized orbitals centered on each atom:

$$\psi_{b\vec{k}}(\vec{r}) = \sum_{\tau j q} e^{i\vec{k} \cdot \vec{R}_{\tau}} C_{jq}^{b\vec{k}} \phi_{jq}(\vec{r} - \vec{R}_{\tau} - \vec{\rho}_j) \quad (2.1)$$

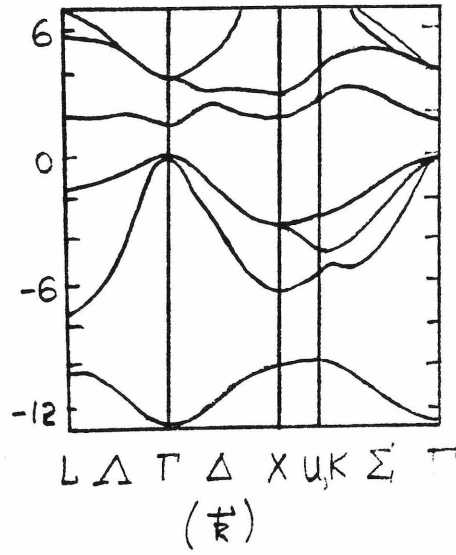
where $\psi_{b\vec{k}}$ is a Bloch wave of momentum \vec{k} and band b , τ labels the unit cells and \vec{R}_{τ} the translation vectors of the lattice, j identifies the atom within the unit cell and $\vec{\rho}_j$ is its location relative to some origin in the cell, ϕ_{jq} represent localized functions on atom j with quantum numbers q , and $C_{jq}^{b\vec{k}}$ are coefficients to be determined by solving Schrödinger's equation. In bulk zincblende crystals, there are two atoms per unit cell and \vec{k} is restricted to a three-dimensional Brillouin zone. We assume the overlap of two ϕ -functions on separate sites to be negligible. In that case the orthonormality of the Bloch waves requires

Figure 2.1. Bulk band structures for GaAs. (a) Nonlocal pseudopotential band structure from Ref. 2; (b) tight-binding band structure from Ref. 14; (c) first Brillouin zone and symmetry points for zinc blende crystals.

a)



b)



c)

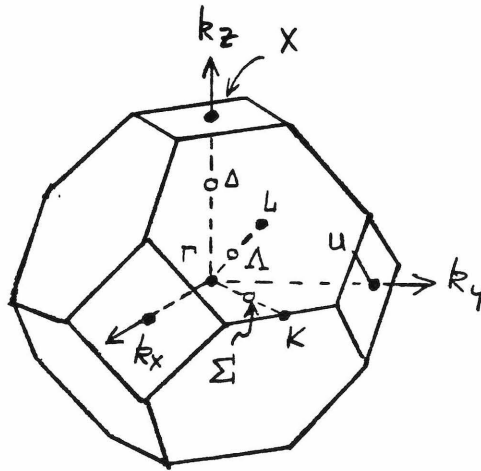


Figure 2.1

$$\sum_{jq} (C_{jq}^{b'k})^* C_{jq}^{bk} = \delta_{b'b} \quad .$$

Schrödinger's equation for $\psi_{b\vec{k}}$ is

$$(H - E_{b\vec{k}}) \psi_{b\vec{k}} = 0$$

If we multiply this by $e^{-i\vec{k}\cdot\vec{R}_\tau} \phi_{j'q'}^*(\vec{r} - \vec{R}_\tau - \vec{\rho}_{j'})$

and integrate over r , we get

$$\sum_{jq} [H_{j'q',jq}(\vec{k}) - E_{b\vec{k}} \delta_{j'q',jq}] C_{jq}^{b\vec{k}} = 0 \quad (2.2)$$

with

$$H_{j'q',jq}(\vec{k}) \equiv \sum_{\tau} e^{i\vec{k}\cdot(\vec{R}_\tau - \vec{R}_{\tau'})} \langle \phi_{j'q'}(\vec{r} - \vec{R}_\tau - \vec{\rho}_{j'}) | H | \phi_{jq}(\vec{r} - \vec{R}_{\tau'} - \vec{\rho}_{j'}) \rangle$$

(2.3)

being the Hamiltonian reduced by translation symmetry. One can see from the matrix equation (2.2) that the number of bands at a given

\vec{k} is equal to the number of basis functions in a unit cell. For our work we use one s- and three p-like states, not including spin, on each atom. In bulk, then, since there are two atoms per unit cell, we have (without spin) eight bands. This is adequate for our work. Certainly high accuracy would require a better basis set, but for the energy range of interest we can make this restriction.

The 8x8 matrix $H(\vec{k})$ representing the reduced bulk Hamiltonian in our restricted basis contains an adequate description of band energies and Bloch states near the fundamental band gap. To evaluate this matrix directly from first principles would be time-consuming and not in keeping with our intentions. Rather, we can choose to take the terms

$$\langle \phi_{j,q}(\vec{r}-\vec{R}_\tau, -\vec{\rho}_{j,q}) | H | \phi_{j,q}(\vec{r}-\vec{R}_\tau, -\vec{\rho}_{j,q}) \rangle$$

to be parameters, and adjust them to fit the band structure shown in Fig. (2.1a). The lowest conduction bands along the Δ direction appear to have an important second Fourier component, and this can be provided by second nearest neighbor terms. Dropping all terms beyond second nearest neighbor ones in Equation (2.3) leaves 19 parameters in zinc blende materials. With certain bounds on the parameters to keep them physically reasonable, one can produce a good approximation to the band structure in Fig. (2.1).

Before describing the procedure for finding the best set of tight-binding parameters, we first mention that in some cases, such

as GaSb, the spin-orbit splitting of the valence band is nearly as large as the band gap and so cannot be neglected in the procedure described above. To include spin, one augments the wave function in Eq. (2.1) to include spinor components. This produces a 16x16 reduced Hamiltonian matrix similar to that in Eq. (2.3). In the absence of spin-orbit splitting, the 16x16 matrix involves the 8x8 matrix and an identical copy, with no interactions connecting them, so the eigenvalues are just those of the 8x8, doubled. Spin-orbit interaction can be naturally included in (2.3), where we assume that such interaction is negligible unless the two localized functions are on the same atom. This is equivalent to replacing the six p states on each atom with four $p_{3/2}$ and two $p_{1/2}$ states, and again the eigenvalues are doubled. (The doubling is required by time reversal symmetry, with or without spin-orbit splitting.) We thus have two additional parameters, reflecting the spin-orbit interactions of each atom.

The fit shown in Fig. (2.1b) was produced by matching the eigenvalues of the matrix Eq. (2.3) to the band structure in Fig. (2.1a) at the high-symmetry points Γ , X, and L. The eigenvalues at X and Γ were constrained to have the proper ordering of the various symmetries. The diagonal, k-independent terms, which represent the atomic state energies, were required to be similar to the energies

from atomic calculations. The first and second nearest neighbor interactions were constrained to have the proper sign, and be roughly the size expected. With all these restrictions, the space takes on very convoluted boundaries. The optimization of the tight-binding parameters with these constraints was carried out by a constrained simplex algorithm⁽⁶⁾. The object is to minimize the function

$$f(\{t\}) = \left[\sum_i W_i (E(\{t\})_i - \epsilon_i)^2 \right] / \sum_i W_i$$

where $E(\{t\})_i$ are some eigenvalues of the Hamiltonian with the set of parameters $\{t\}$, ϵ_i are the energies to be fit, and W_i is some weight. Initial guesses were generated by setting second nearest neighbor parameters to zero, which allows simple analytic solutions of $E(\{t\})$ at certain points. It was sometimes necessary to fit additional points along the Δ and Λ directions. Convergence and uniqueness were checked by changing the search parameters and initial guess.

The parameters obtained by the above prescription for a variety of semiconductors are shown in Table 2.1. The on-site energies (the first four) have common zero which is determined by setting to zero the energy of the valence band maximum of the resulting band structure. The original band structures for GaAs, GaSb, GaP, InP, InAs, ZnSe, and CdTe were taken from Ref. (2). The ZnTe band structure was obtained from Ref. (7). Reference (8) was the source of the AlAs band structure.

Table 2.1. Tight-binding parameters for several III-V and II-VI parameters. The notation is that of Ref. 4. The subscripts 0 and 1 designate anion and cation, respectively. Δ is the spin-orbit strength. All parameters are in units of eV. The zero of energy is the valence band maximum. The GaAs parameters are from Ref. 14. All others were obtained by M. S. Daw and D. L. Smith.

	<u>GaAs</u>	<u>AlAs</u>	<u>InAs</u>	<u>GaP</u>	<u>InP</u>	<u>GaSb</u>	<u>ZnTe</u>	<u>CdTe</u>	<u>ZnSe</u>
1. $E_{SS}(000)_0$	-6.953	-6.698	-7.039	-7.394	-7.214	-6.198	-7.605	-8.905	-8.110
2. $E_{SS}(000)_1$	-2.254	-0.754	-1.815	-1.918	-0.737	-2.536	2.004	1.703	1.310
3. $E_{XX}(000)_0$	1.338	1.413	0.770	1.027	1.171	1.313	1.676	0.703	0.134
4. $E_{XX}(000)_1$	1.839	1.999	1.453	2.005	2.044	3.093	3.308	3.935	5.751
5. $E_{SS}(\frac{1}{2}\frac{1}{2}\frac{1}{2})$	-1.774	-1.743	-1.226	-1.913	-1.241	-1.602	-0.609	-0.224	-1.550
6. $E_{SX}(\frac{1}{2}\frac{1}{2}\frac{1}{2})_{01}$	1.304	1.150	1.416	1.288	1.265	1.182	1.381	0.768	0.480
7. $E_{SX}(\frac{1}{2}\frac{1}{2}\frac{1}{2})_{10}$	1.121	1.038	1.182	1.261	1.173	1.127	1.070	0.973	1.420
8. $E_{XX}(\frac{1}{2}\frac{1}{2}\frac{1}{2})$	0.479	0.509	0.407	0.598	0.495	0.206	0.570	0.459	0.745
9. $E_{XY}(\frac{1}{2}\frac{1}{2}\frac{1}{2})$	1.447	1.193	1.107	1.231	1.195	1.478	1.289	1.125	1.388
10. $E_{XY}(110)_0$	0.295	0.308	0.188	0.256	0.168	0.055	0.324	0.001	0.425
11. $E_{XY}(110)_1$	0.195	0.111	0.302	0.086	0.228	0.010	0.000	0.142	0.040
12. $E_{XX}(110)_0$	0.200	0.230	0.155	0.247	0.226	0.072	0.224	0.087	0.337
13. $E_{XX}(110)_1$	0.207	0.223	0.316	0.286	0.242	0.222	0.292	0.140	0.108
14. $E_{XX}(011)_0$	-0.347	-0.506	-0.316	-0.395	-0.462	-0.492	-0.638	-0.255	-0.381
15. $E_{XX}(011)_1$	-0.282	-0.101	-0.112	-0.072	-0.125	-0.365	0.000	-0.046	-0.166
16. $E_{SX}(110)_0$	0.001	0.000	0.001	0.001	0.002	0.158	0.000	0.106	0.129
17. $E_{SX}(110)_1$	0.018	0.003	0.011	0.022	0.000	0.172	0.000	0.000	0.000
18. $E_{SS}(110)_0$	-0.002	-0.072	-0.267	-0.001	-0.166	-0.032	-0.260	-0.319	-0.085
19. $E_{SS}(110)_1$	-0.178	-0.034	-0.001	-0.052	0.000	-0.177	0.000	-0.014	-0.146
20. Δ_0	-----	-----	-----	-----	-----	0.265	-----	0.347	0.174
21. Δ_1	-----	-----	-----	-----	-----	0.017	-----	0.013	0.021

Table 2.1

The calculations for the (110) surface band structure were performed in the manner used for bulk bands, except that now we describe the surface by using a finite slab of atoms. The crystal momentum parallel to the surface is a conserved quantity and is used to label the states. The unit cell now consists of a volume which stretches from one surface to the other. The slab is thick enough to isolate the opposite surfaces from each other, this thickness being nine atomic layers. The surface geometry is taken to be that suggested by LEED results ⁽¹²⁾, when available, and from energy minimization calculations ⁽¹³⁾ when LEED results have not been obtained. The tight-binding parameters at the surface are linear combinations of the bulk parameters, analogous to the transformation of components of a rotated vector modulated by a d^{-2} scaling relation. The scaling had little effect on the results because nearest neighbor bond lengths are constant to within 3%. Prior to relaxation, occupied As-derived and empty Ga-derived surface states occur in the band gap. The surface relaxation pushes the Ga-derived states into the conduction band and the As-derived states into the valence band.

The relaxed (110) GaAs surface band structure produced by our tight-binding method is shown in Fig. (2.2). The energy is relative to the valence band maximum at 0. Surface states can be identified near the valence band maximum and the conduction band minimum. These states have low dispersion and are removed from the valence and conduction bands at the M point. These states are largely the As and Ga dangling bonds.

Figure 2.2. The band structure of a slab of GaAs. The slab is nine layers thick along the (110) direction. The structure is from the tight-binding Hamiltonian discussed in the text.

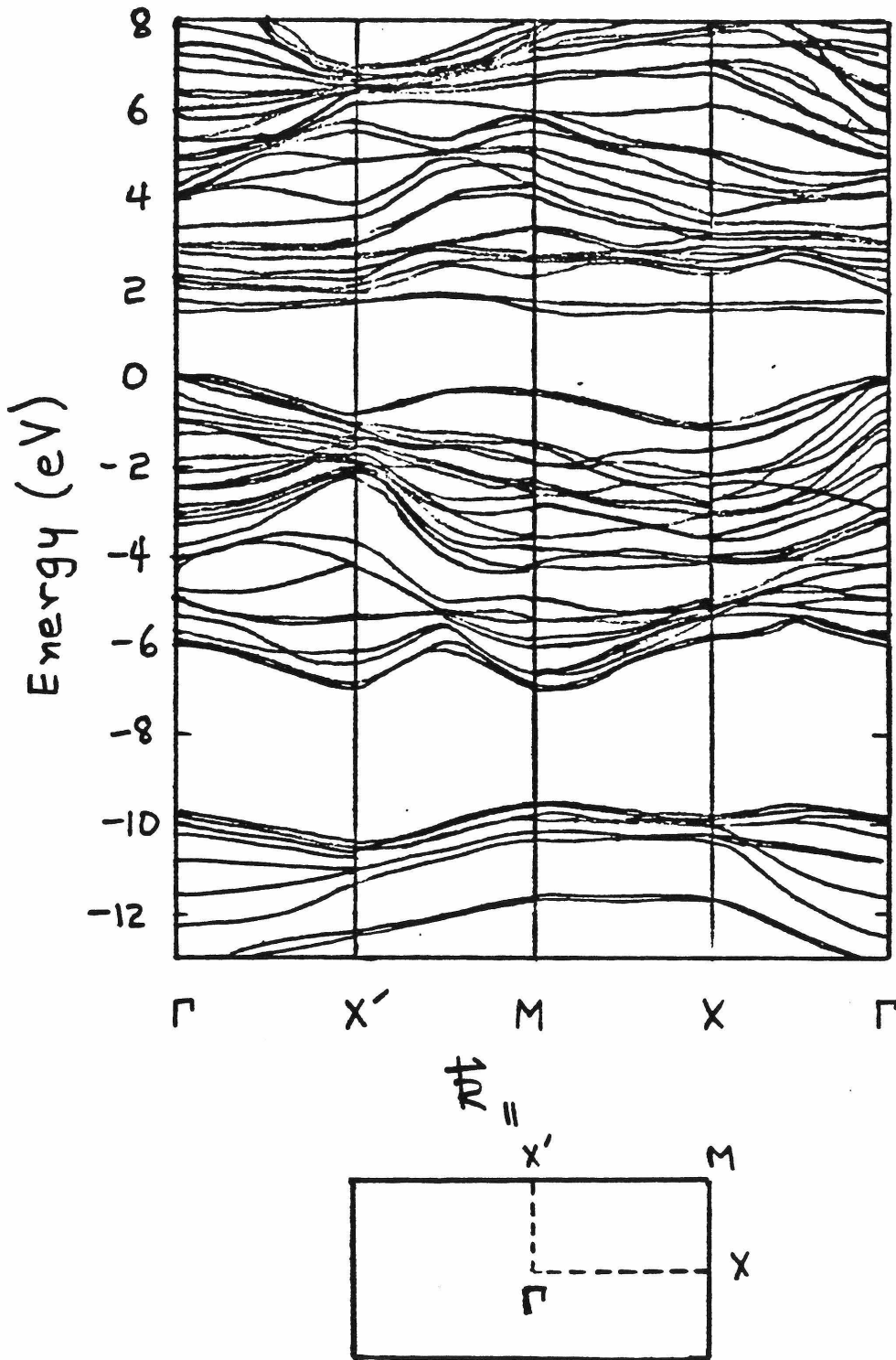


Figure 2.2

III. GREEN'S FUNCTION IN SEMICONDUCTORS

Now that we have devised a means for handling the electronic states in the perfect crystal, we treat the case where some modification is added, represented by a potential $V_d(r)$ that vanishes as $r \rightarrow \infty$. Schrödinger's equation is now

$$[H_0 + V_d] \xi(r) = \epsilon \xi(r)$$

where H_0 is the perfect crystal Hamiltonian for bulk or slab. Following the treatment developed in Ref. 9, we have

$$[1 - \hat{G}_+(\epsilon) \hat{V}_d] \xi = \psi$$

where ψ represents an incoming Bloch wave and ξ is the complete solution including incoming wave and some outgoing scattered wave.

The Green's function is defined by

$$\hat{G}_+(\epsilon) = \lim_{\delta \rightarrow 0^+} (\epsilon + i\delta - \hat{H}_0)^{-1} \quad (2.4)$$

For bound states, we have

$$[1 - \hat{G}_+(\epsilon) \hat{V}_d] \xi = 0 \quad . \quad (2.5)$$

The solutions are obtained by tracing out the eigenvalues of $[1 - \hat{G}_+(\epsilon) \hat{V}_d]$ and finding when one or more cross zero. The function ξ is then the appropriate eigenfunction, given $(\xi|\xi) = 1$. We label

the various solutions by ϵ_β and ξ_β .

We expand ξ in terms of localized functions, as we expanded the Bloch waves in Eq. (2.1):

$$\xi(\vec{r}) = \sum_{\tau j q} D_{\tau j q} \phi_{j q}(\vec{r} - \vec{R}_\tau - \vec{\rho}_j) \quad (2.6)$$

Then Eq. (2.5) becomes

$$\sum_{\tau j q} [\delta_{j' j} \delta_{q' q} \delta_{\tau' \tau} - (G + (\epsilon) V_d)_{\tau' j' q', \tau j q}] D_{\tau j q} = 0 \quad (2.7)$$

If V_d can be taken as localized in this basis, then Eq. (2.7) can be solved in practical fashion. In particular, suppose that V_d can be restricted to the set of functions localized on one lattice site, call it 0. Then

$$(V_d)_{\tau' j' q', \tau j q} = \delta_{\tau' 0} \delta_{j' 0} \delta_{\tau 0} \delta_{j 0} v_{q' q} \quad (2.8)$$

In this case, Eq. (2.7) separates into two equations, one for $j' = 0$, $\tau' = 0$ and one for $j' \neq 0$, $\tau' \neq 0$. If we call

$$d_q = D_{00q} \quad ,$$

then

$$\sum_q [1 - g_+(\varepsilon) v]_{q'q} d_q = 0 \quad (2.9)$$

$$D_{\tau'j'q'} = \sum_{q''q} G_+(\varepsilon)_{\tau'j'q',ooq''} v_{q''q} d_q \quad (2.10)$$

where

$$g_+(\varepsilon)_{q'q} = G_+(\varepsilon)_{ooq',ooq} \quad (2.11)$$

Equation (2.9) now fixes ε and d_q (to within a normalization factor). We take one s and three p functions on each atom in our basis, so this equation involves a 4x4 matrix. Once the energies ε_β and d_q^β are found, Eq. (2.10) gives the rest of the wave function, and $(\xi|\xi) = 1$ fixes the normalization factor. The matrix g_+ and the solutions depend strongly on the chosen site 0. This is implicit in what follows.

We come now to evaluating the Green's function. To find the energies ε_β , we need

$$g_+(\varepsilon)_{qq'} = \sum_{\vec{b}\vec{k}} \frac{C_{oq}^{\vec{b}\vec{k}} C_{oq'}^{\vec{b}\vec{k}*}}{\varepsilon^+ - E_{\vec{b}\vec{k}}} \quad , \quad (2.12)$$

where the C's and E's come from solutions to Eq. (2.2). Symmetry

can clearly be used to reduce the sum. It is convenient to form the set of all rotations R such that $E(b\vec{k}) = E(b(\hat{0}_R\vec{k}))$. These form the operations of the point group and are characteristic of the lattice. It is then convenient to set the localized functions into symmetrized linear combinations transforming like irreducible representations of the group, where the origin for the rotations is chosen to be the center of the potential V . By manipulations, the sum over the set of \vec{k} can then be reduced to a fraction of that set.

Time-reversal symmetry reduces the sum by another factor of two. For bulk zinc blende crystals, we need effectively only evaluate 1/48th of the full Brillouin zone. For example,

$$(p_x | g_+ | p_x) = 48 [(p_x | g^r | p_x) + (p_y | g^r | p_y) + (p_z | g^r | p_z)] 1/3$$

where g^r is like g_+ in Eq. (2.12), except that the sum over k is restricted to 1/48th of the zone. Near the surface, 1/4th of the two-dimensional zone is required. One can also use translation symmetry to speed convergence of the sum for the non-singular part of g ⁽¹¹⁾. The number of points in the integration over \vec{k} was increased until the solutions ϵ of Eq. (2.9) discussed in Chapters 3 and 4 converged to within 0.1 eV.

In bulk, g_+ is diagonal in the s-p basis. The diagonal elements

for the three p-states are identical. This leaves four independent elements: $(g_+)_{SS}$ for s-states and $(g_+)_{XX}$ for p-states on cation and anion. The four elements for bulk GaAs are shown in Fig. (2.3) for energies in the band gap, where their imaginary parts vanish.

Near the surface, $g_+(\epsilon)$ is no longer diagonal in the s-p basis. We diagonalize $g_+(\epsilon)$ by a unitary transformation $u(\epsilon)$. Each column of $u(\epsilon)$ defines a linear combination of s and p states on the given site which is (within the basis) an eigenvector of $\hat{g}_+(\epsilon)$. These columns are labelled $\alpha^{(+)}(\epsilon)$, $\tau_D^{(+)}(\epsilon)$, $\tau_B^{(+)}(\epsilon)$, and $\tau_T^{(-)}(\epsilon)$, where the sign indicates the parity of the specified combination of functions under the mirror symmetry of the (110) surface. The elements of g_+ when diagonalized are $(\alpha^{(+)}(\epsilon)|g_+(\epsilon)|\alpha^{(+)}(\epsilon))$, and $(\tau_D^{(+)}(\epsilon)|g_+(\epsilon)|\tau_D^{(+)}(\epsilon))$, $(\tau_B^{(+)}(\epsilon)|g_+(\epsilon)|\tau_B^{(+)}(\epsilon))$, and $(\tau_T^{(-)}(\epsilon)|g_+(\epsilon)|\tau_T^{(-)}(\epsilon))$. These we call $\tilde{g}_{\alpha\alpha}$, \tilde{g}_{DD} , \tilde{g}_{BB} , and \tilde{g}_{TT} , respectively. Loosely speaking, the \tilde{g}_{SS} bulk element goes into the $\tilde{g}_{\alpha\alpha}$ element as one approaches the surface, while the degenerate g_{XX} elements split to form the \tilde{g}_{DD} , \tilde{g}_{BB} , and \tilde{g}_{TT} .

The four components of \tilde{g} , the diagonalized form of g , are plotted for surface Ga and As atoms in Figs. (2.4) and (2.5) for (110) GaAs. The \tilde{g}_{DD} elements in both figures are obviously different from the other components and from the bulk components in Fig. (2.2). These functions show a major effect of the dangling bonds on the Green's function.

Figure 2.3. The diagonal elements of the Green's function in bulk GaAs. The g_{xx} refers to the elements between the same p-functions.

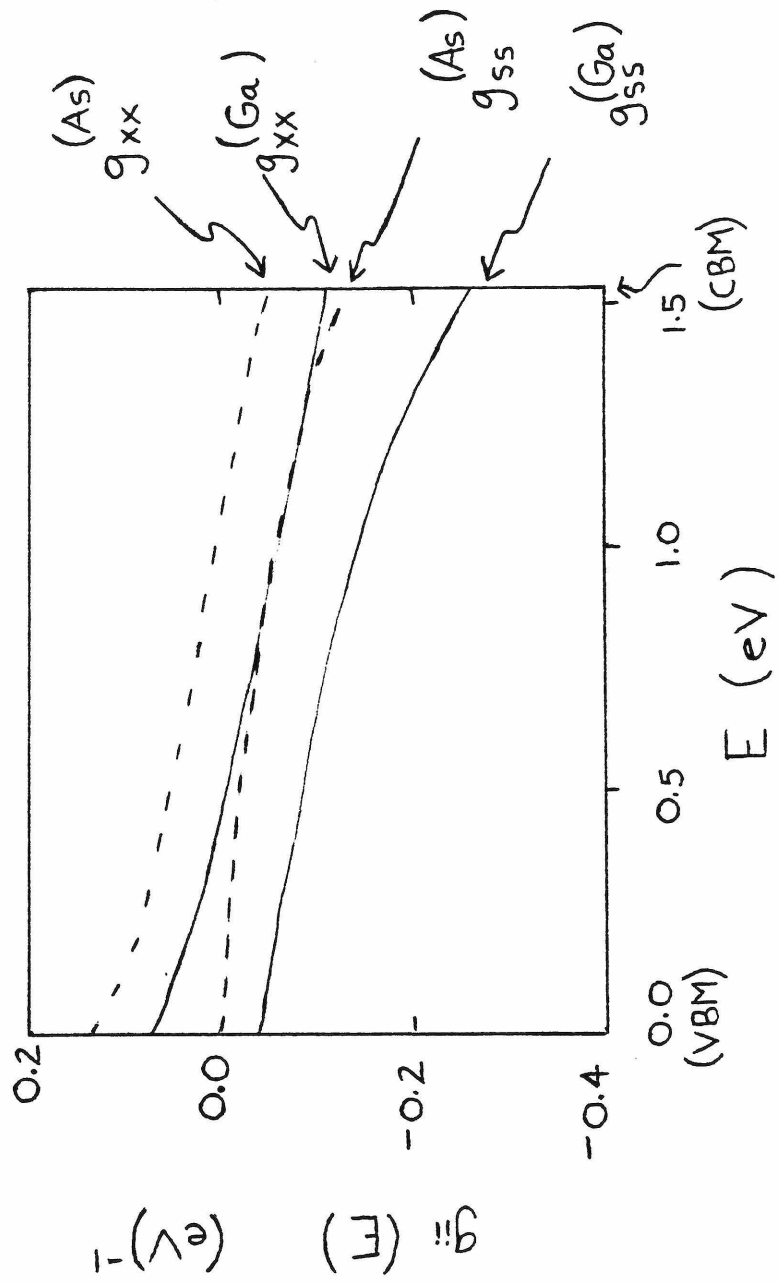


Figure 2.3

Figure 2.4. The components of \tilde{g} on Ga atoms in the (110) surface of GaAs. The notation is explained in the text.

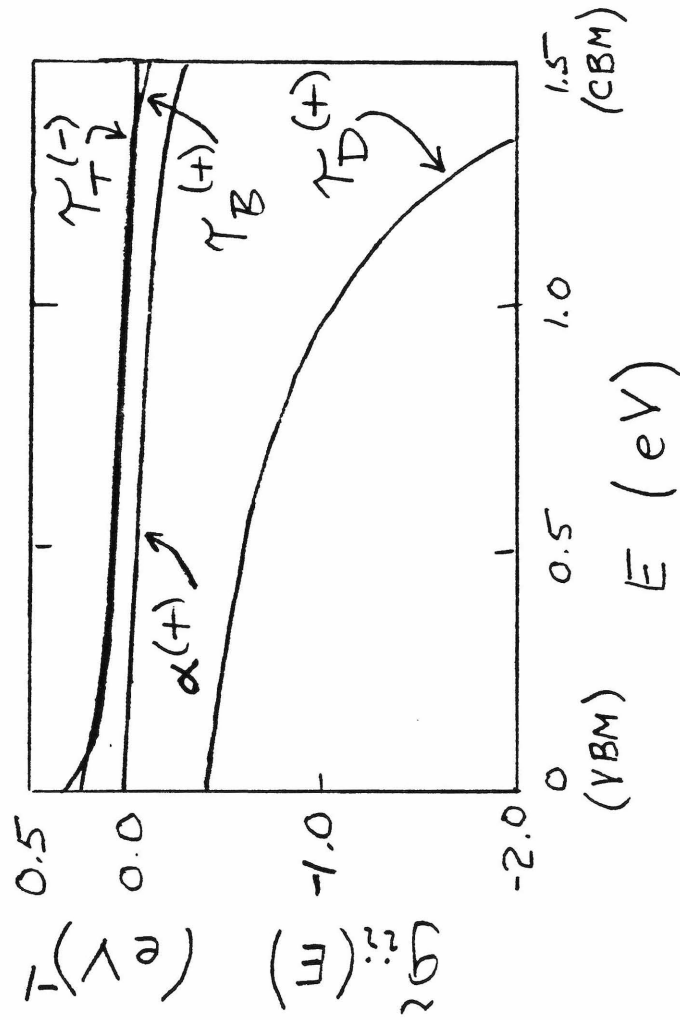


Figure 2.4

Figure 2.5. The components of \tilde{g} on As atoms in the (110) surface of GaAs. The notation is explained in the text,

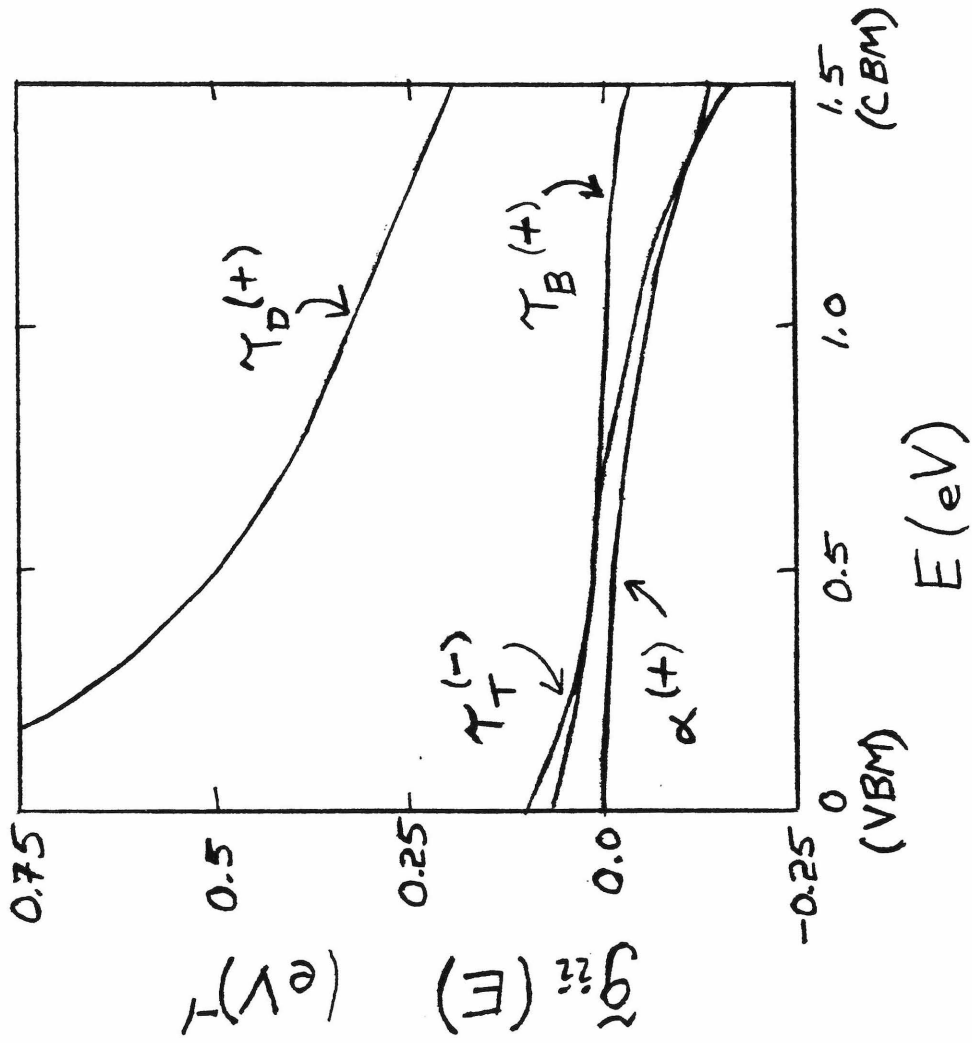


Figure 2.5

The role of the surface states can be demonstrated by examining the form of \tilde{g} . In the gap, g has the form

$$g(\epsilon)_{\ell m} = P \int_{-\infty}^{\infty} ds \frac{n(s)_{\ell m}}{\epsilon - s} \quad (2.8)$$

where P indicates the principal part, and where the density of states matrix is

$$n(s)_{\ell m} = \sum_{\vec{b}\vec{k}} C_{0\ell}^{\vec{b}\vec{k}} C_{0m}^{\vec{b}\vec{k}*} \delta(s - E_{\vec{b}\vec{k}}) \quad (2.9)$$

The site 0 may be in bulk or near the surface.

Then, for instance

$$\begin{aligned} \tilde{g}_{\alpha\alpha}(\epsilon) &= (\alpha^{(+)}(\epsilon) | g(\epsilon) | \alpha^{(+)}(\epsilon)) \\ &= P \int_{-\infty}^{\infty} ds \frac{(\alpha^{+}(\epsilon) | n(s) | \alpha^{+}(\epsilon))}{\epsilon - s} \end{aligned} \quad (2.10)$$

where $\alpha^{+}(\epsilon)$ is one of the columns of $u(\epsilon)$, which diagonalizes $g(\epsilon)$.

The numerator of the foregoing integrand represents the contribution to the density of states due to one particular state. This we call a partial density of states.

We plot in Fig. (2.6) the partial densities of states for $\tau_D^{(+)}$ and $\tau_T^{(-)}$ on Ga and As atoms in bulk and on the surface. The states $\tau_D^{(+)}$ and $\tau_T^{(-)}$ are fixed by finding where the corresponding diagonal element of \tilde{g} vanishes, i.e., $(\tau_D^{(+)}(\epsilon) | g(\epsilon) | \tau_D^{(+)}(\epsilon)) = 0$

Figure 2.6. Partial density of states for the $\tau_D^{(+)}$ and $\tau_T^{(-)}$ states near the (110) GaAs surface. The corresponding bulk (p or t_2 orbital) partial density of states is also shown.

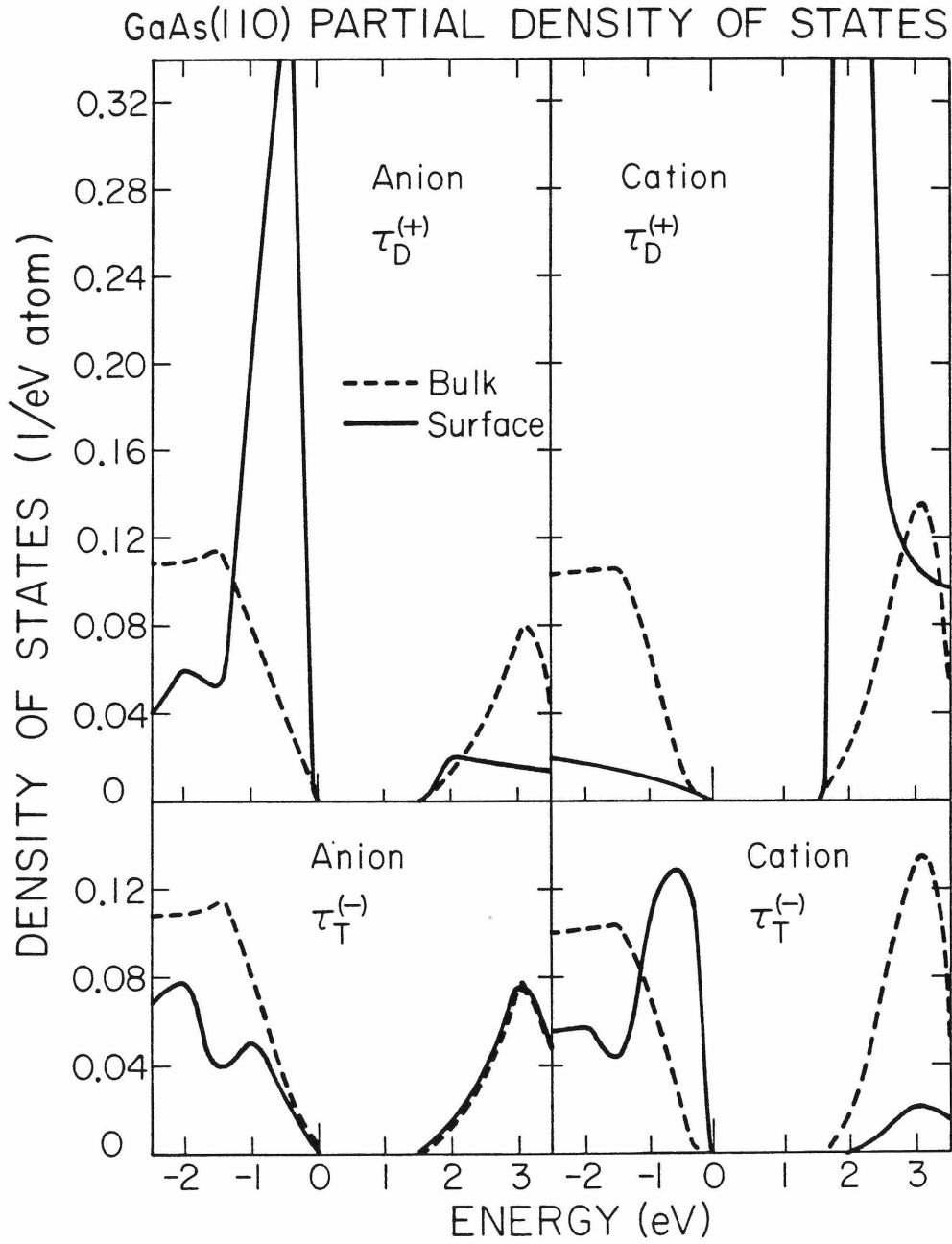


Figure 2.6

or $(\tau_T^{(-)}(\epsilon) | g(\epsilon) | \tau_T^{(-)}(\epsilon)) = 0$. Clearly the $\tau_D^{(+)}$ partial density has sharp resonances near the surface. These are the Ga and As dangling bond states. The $\tau_T^{(-)}$ partial density changes less, because the dangling bonds have positive parity and $\tau_T^{(-)}$ has negative.

Thus the large surface state resonances push the $\tau_D^{(+)}$ functions far away from their bulk values. The other functions change near the surface, but not by as much.

Having calculated $g_+(\epsilon)$ in bulk and near the surface, we may proceed to find bound states due to some potential V , as prescribed by Eq. (2.5). This is done in the next two chapters for core excitons and vacancies.

IV. SUMMARY

This chapter presents a realistic, second nearest neighbor tight-binding Hamiltonian for bulk and surface band structure calculations. The wave functions are expanded in a set of localized orbitals and the matrix elements of the Hamiltonian are treated as adjustable parameters. These parameters are adjusted to fit the bulk band structures of nine zinc blende semiconductors. Band structures for the (110) surfaces of these materials are then calculated.

The states due to an interruption in the periodic potential are then obtained using a Koster-Slater, tight-binding Green's function approach. The Green's function is calculated in bulk and near the (110) surface, in preparation for calculations in Chapter 3 and 4.

REFERENCES

1. F. Bassani and G. Pastori Parravicini, Electronic States and Optical Transitions in Solids (Pergamon Press, New York, 1975).
2. Such as that which is discussed by J. R. Chelikowsky and M. L. Cohen, Phys. Rev. B14, 556 (1976).
3. J. A. Applebaum and D. R. Hamann, Phys. Rev. Lett. 32, 225 (1974).
4. J. C. Slater and G. F. Koster, Phys. Rev. 94, 1498 (1954).
5. S. T. Pantelides, Rev. Mod. Phys. 50, 797 (1978).
6. J. L. Kuester and J. H. Mize, Optimization Techniques with Fortran (McGraw-Hill, New York, 1973), M. J. Box, Computer J. 8, 42 (1965).
7. M. L. Cohen and T. K. Bergstresser, Phys. Rev. 141, 789 (1966).
8. E. Hess, I. Topol, K. R. Schulze, H. Neumann, and K. Unger, Phys. Stat. Sol.(b) 55, 187 (1973).
9. G. F. Koster and J. C. Slater, Phys. Rev. 95, 1167 and 96, 1208 (1954). J. Callaway, J. Math. Phys. 5, 783 (1964) and Phys. Rev. 154, 515 (1967).
10. J. Bernholc and S. T. Pantelides, Phys. Rev. B18, 1780 (1978).
11. H. J. Monkhorst and J. D. Pack, Phys. Rev. B13, 5188 (1976).
12. LEED geometries are available for the (110) surfaces of GaAs, InP, ZnTe, and GaP. See C. B. Duke, R. J. Meyer, and P. Mark, J. Vac. Sci. Technol. 17, 971 (1980) for the first three and C. B. Duke, A. Paton, J. Carelli, and A. Kahn (to be published) for GaP.

13. D. J. Chadi, Phys. Rev. Lett. 41, 1062 (1978) and Phys. Rev. B19, 2074 (1979).
14. G. C. Osbourn and D. L. Smith, Phys. Rev. B19, 2124 (1979).

CHAPTER 3

SURFACE CORE EXCITONS IN SEMICONDUCTORS

I. INTRODUCTION

The existence of surface core excitons was first substantiated by Lapeyre and Anderson in 1975 ⁽²⁾. Their work explained the presence of peaks in some photoemission experiments, such as those in Fig. (1.5a) ⁽¹⁾. These peaks had originally been interpreted as evidence of intrinsic surface states in the gaps of some semiconductors ⁽¹⁾. When Huijser and Van Laar () showed that no such surface states exist on, for example, (110) GaAs, the appearance of the peaks in the gap was then attributed to strong core exciton effects. This was proven by Lapeyre and Anderson, who showed that the peaks in the (110) GaAs surface spectra were definitely related to transitions from the Ga(3d) core to the Ga dangling bond, and that the attraction between core hole and electron must be strong enough to make the transition appear in the gap.

The existence of strongly bound surface excitons was somewhat surprising at first. Bulk core excitons have been observed and well understood ⁽¹³⁾. There the core hole resembles a positive charge in the nucleus, leading to donor-like states. These states are hydrogenic with Bohr radii of typically tens or hundreds of Å's and binding energies of tens of meV. The surface excitons are by contrast very localized, being restricted to mostly one atom, and the binding energies reach nearly 1.0 eV.

Excitons have been observed by exciting the Ga(3d) level in (110) GaAs, GaP, and GaSb and the In(4d) level in (110) InP^(1,3,4,6,7,8,9). Reports of p-core excitons have been absent. Some authors have searched and concluded that no excitonic transitions are observable from those cores^(5,7).

The situation with anion surface core excitons is obscured somewhat. The best data are available for (110) GaAs. The As(3d) to Ga dangling bond transition has been observed as a resonance with transitions to the conduction band⁽⁹⁾, so excitonic effects are much smaller than for the cation core transitions. Only one observation of an As(3p) transition has been reported, and this appears to have very large binding energy⁽⁷⁾. This report was not very complete, and is in contradiction with preliminary results from other experiments⁽¹²⁾.

In the next section, we show theoretically how the electron-hole interaction does produce a bound state for transitions from cation core levels on the (110) surface of III-V semiconductors. The p-core transitions are shown to have weaker oscillator strengths than the d-core transitions, making the former much less observable. We also show that anion core transitions produce no bound states. Detailed comparison to experiment is made.

II. CALCULATION OF BINDING ENERGIES AND OSCILLATOR STRENGTHS

We present here a complete theoretical picture of anion and cation core excitons for III-V surfaces, using relaxed surface geometries. A qualitative picture serves to summarize our concept of surface core excitons. On the (110) surface of III-V's there are two species of dangling bonds: the cation dangling bond, which because of surface relaxation is mostly p (3% s) and is empty, and the anion dangling bond which is mostly sp^3 -hybrid and fully occupied. A dipole transition out of a cation d- or s- core level, for example, goes easily to the empty, p-type dangling bond on that atom. The electron in this final state is localized near the hole and the Coulombic attraction produces strong binding. The d- or s-core excitation would have different transition energies, but closely similar binding energies because the potential due to an s-core hole is hardly different from that due to a d-core hole, as viewed by the excited electron.

An excitation out of a cation p-core level would have the same binding energy as s- or d-core excitons, but this transition couples to the small s-component of the dangling bond, reducing the oscillator strength by a factor of about 30 from the cation d-core level transition.

In the case of excitation out of the anion core, the on-site dangling bond is fully occupied and the electron must go to other un-

occupied states, any of which is less localized. One would for this reason expect less binding for surface anion core excitons than for the cation excitation. We thus find a sharp contrast between anion and cation surface core excitations.

The calculations were based on the Koster-Slater approach in the tight-binding approximation, discussed in Chapter 2. We start with the condition for a bound state, from Eq. (2,9),

$$\det |1 - g_+(\epsilon) v| = 0 \quad (3.1)$$

where v represents the potential due to the exciton. We approximate v by considering that the core hole is very localized compared to the valence electrons and so the potential for the excited electron in the localized basis should resemble that for the valence electrons of the next heaviest element. We can then take

$$\langle \phi_\alpha | v | \phi_\beta \rangle = \delta_{\alpha\beta} [E_\alpha(z+1) - E_\alpha(z)] \quad (3.2)$$

where $E_\alpha(z)$ is the energy of state α on the atom with nuclear charge z , as culled from atomic calculations. Values for v_α are shown in Table 3.1.

In Table 3.2 we present our results for binding energies and oscillator strengths. The cation p and d core excitations on GaAs, GaP, and InP are seen to be bound strongly. The Ga core excitations on GaSb are bound weakly with respect to the conduction band minimum. We find no binding for any of the anion core excitations. We find

Table 3.1. Values of the core exciton potentials for Ga, In, P, As, and Sb. The potentials are defined in the text. Atomic energy levels come from Ref. 11.

TABLE 3.1

Atom	v_{ss} (eV)	v_{pp} (eV)
Ga	-3.0	-1.5
In	-2.4	-1.2
P	-3.7	-2.0
As	-3.0	-1.6
Sb	-2.3	-1.3

Table 3.2. Theoretical and experimental binding energies of surface core excitons on (110) GaAs, GaP, InP, and GaSb. Oscillator strengths for excitons are also calculated and normalized to the d-core strength. References for the data follow.

- a) Ref. 1
- b) Ref. 3
- c) Ref. 4
- d) Ref. 5
- e) Ref. 6
- f) Ref. 7
- g) Ref. 8
- h) Ref. 9
- i) Ref. 12

TABLE 3.2

Theory

Material	Core	Binding Energy (eV)	Oscillator Strength (relative to d)	Experiment Binding Energy (eV)
GaAs	Ga(3p)	0.9	3%	— d,f
	Ga(3d)	0.9	100%	0.8 ^a , 0.6 ^b , 0.5 ^e , ≈0.4 ^f , ≥0.8 ^g , 1.3 ^h
	As(3p)	<0		≈1.5 ^f , — ⁱ
	As(3d)	<0		— d,f,g, -0.7 ^h
GaP	Ga(3p)	0.8	3%	
	Ga(3d)	0.8	100%	1.45 ^b , 1.1 ^e , 0.8 ^g
	P(2p)	<0		
InP	In(4p)	0.6	3%	
	In(4d)	0.6	100%	0.3 ^c , 0.4 ^e
	P(2p)	<0		
GaSb	Ga(3p)	≈0	3%	
	Ga(3d)	≈0	100%	0.2 ^b , 0.1 ^e , 0.7 ^g
	Sb(4p)	<0		
	Sb(4d)	<0		— ^g

that these states occur in the conduction band. We also present the oscillator strengths relative to the d-core exciton for deeply bound excitons. In GaAs, GaP, and InP, we see that the cation p-core transition is more than an order of magnitude weaker than the cation d-core, though they have the same binding. This difference in magnitude reflects the small s-character of the cation dangling bond.

Also in the table we present binding energies published from separate experiments. In general, though the reported binding energies show some disagreement between experiments, there is good agreement between most of the data and our calculated binding energies. Also, the reports show no observed transition for cation p-core excitations, in agreement with the predicted relative oscillator strengths.

Anion core excitons have not been reported except for a rather incomplete description by Bauer, et al ⁽⁵⁾ of an observed As(3p) exciton on GaAs with binding on the order of the band gap. This observation contradicts our picture of surface core excitons. For a surface As(3p) electron to be promoted to a dangling bond, it must end up principally on the neighboring surface Ga dangling bonds, and the resulting separation between hole and electron is larger than in the case of a Ga core exciton where the electron can reside on the same atom as the hole. The resulting larger separation for the As excitation lowers the Coulombic interaction and, one would expect,

also the binding energy. One would believe that the As excitons would have less binding, not more, than the Ga exciton. The reported As(3p) exciton is clearly in contradiction with this theory.

Preliminary results from other experiments have indicated that no As(3p) exciton is present (12).

Our calculations are confirmed somewhat by calculations by Swarts, Goddard, and McGill (10). They calculate for clusters of surface atoms the transition energies of various core excitations and the nature of the electron's final state. The anion excitation is less bound than the cation exciton, in agreement with our results. They show that the final state for the electron excited from an anion core is mostly (>90%) composed of neighboring surface Ga dangling bonds. This holds despite the inclusion of additional states centered on the arsenic which would allow for the electron to pull closer to the hole. They also note the discrepancy with Bauer's reported As(3p) exciton.

The uniqueness of the Ga dangling bond state on (110) GaAs can be seen clearly in Fig. (3.1). Here are plotted solutions of Eq. (2.5) for $v_{ss} = v_{pp} = v$. The error in neglecting the difference between v_{ss} and v_{pp} is not large for our problem. One can see immediately that there is a state which binds for $|v| < 5$ eV when the potential is centered on a surface Ga atom. This is mostly formed from the Ga dangling bond. Our definition puts $v \approx -1.5$ eV for core excitations on both Ga and As. The binding energy for the

Figure 3.1. Core exciton binding energies in GaAs for $v_{ss} = v_{pp}$. Surface states are in the (110) surface. Ga and As refer to the position of the core hole.

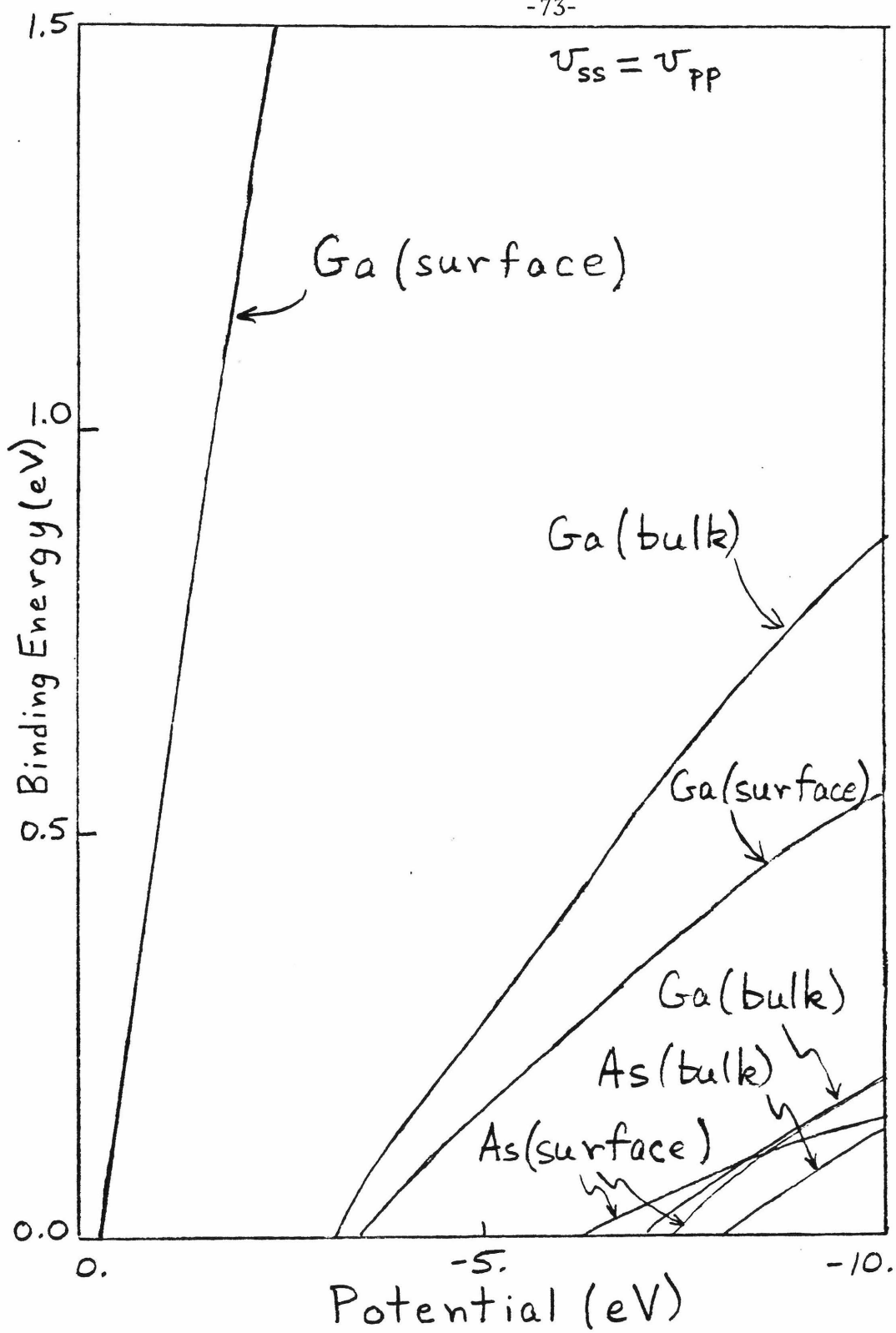


Figure 3.1

Ga(3d) exciton is thus estimated to be about 0.8 eV, close to the value shown in Table 3.2. The binding energy is clearly sensitive to the values of $v_{\alpha\beta}$. It is also evident that no bound states are produced for a potential centered on a surface As atom for $|v| < 6$ eV. To get a binding energy of ≈ 1.5 eV for such a state would require $v \approx -500$ eV! In light of this, one sees that the reported As(3p) exciton cannot be explained by refining the values of $v_{\alpha\beta}$.

In light of the theoretical evidence against the existence of the As(3p) surface exciton in GaAs, and for lack of confirmation from other experiments, we conclude that transitions from anion cores on III-V surfaces do not lead to excitons.

In conclusion, the calculated surface core excitonic binding energies appear to be in good agreement with the data in all but one case. The report of the As(3p) exciton has not been confirmed by another experiment, and may yet prove to be in error. The computed oscillator strengths explain why cation d-core excitons are seen when no p-core transitions are observed.

III. SUMMARY

This chapter presents a complete theoretical picture of anion and cation core excitons in III-V surfaces, using the Koster-Slater, tight-binding Green's function technique, discussed in Chapter 2. The nature of surface core excitons is shown to be closely related to the cation dangling bonds. Binding energies and relative oscillator strengths are calculated and comparison is made with experiment. The localization of the electron to the same atom as the core hole produces large binding for cation core transitions. Anion core transitions are shown to have no binding. Cation p-core transitions are shown to be damped relative to d-core transitions due to weak oscillator strengths.

REFERENCES

1. D. E. Eastman and J. L. Freeouf, Phys. Rev. Lett. 33, 1601 (1974).
2. G. J. Lapeyre and J. Anderson, Phys. Rev. Lett. 35, 117 (1975).
3. D. E. Eastman and J. L. Freeouf, Phys. Rev. Lett. 34, 1624 (1975).
4. W. Gudat and D. E. Eastman, J. Vac. Sci. Technol. 13, 831 (1976).
5. R. S. Bauer, R. Z. Bachrach, S. A. Flodstrom, and J. C. McMenamin, J. Vac. Sci. Technol. 14, 378 (1976).
6. J. Van Laar, A. Huijser, and T. L. van Rooy, J. Vac. Sci. Technol. 14, 894 (1977).
7. R. S. Bauer, D. J. Chadi, J. C. McMenamin, and R. Z. Bachrach, Proc. 7th Intern. Vac. Congr. and 3rd Intern. Conf. Solid Surfaces, Vienna 1977, edited by R. Dorbrozensky, et al, (Technische Universität Wien, Vienna, 1977), p. A-2699.
8. D. E. Eastman, T.-C. Chiang, P. Heimann, and F. J. Himpsel, Phys. Rev. Lett. 45, 656 (1980).
9. P. Zürcher, G. J. Lapeyre, and R. Avci, J. Vac. Sci. Technol. (to be published).
10. C. A. Swarts, W. A. Goddard, III, and T. C. McGill, J. Vac. Sci. Technol. (to be published).

11. F. Herman and S. Skillman Atomic Structure Calculations,
(Prentice-Hall, New Jersey, 1963).
12. P. Zürcher, private communication.
13. M. Altarelli, Journ. de Phys., 39, C4-112 (1978).
14. A. Huijser and J. Van Laar, Surf, Sci, 52, 202 (1975).

CHAPTER 4

VACANCIES NEAR SEMICONDUCTOR SURFACES

I. INTRODUCTION

This chapter presents the first realistic calculation, to our knowledge, of deep levels near the surface of semiconductors. The study of deep levels in the bulk has advanced only to the stage of qualitative accuracy ⁽¹⁾, and the calculation for levels near the surface is similarly primitive. Yet there is a great deal of interest in these states, and much can be learned from the results presented here.

We begin by treating in the next section the levels of an ideal vacancy in bulk. We use the tight-binding Koster-Slater ^(3,4) approach from Chapter 2 to calculate the states due to ideal vacancies in the bulk of a variety of III-V and II-VI semiconductors. Even though we ignore the Jahn-Teller effect ⁽²⁾ and Coulomb repulsion among bound electrons in the treatment of ideal vacancies, many of the qualitative aspects of ideal vacancies hold for real vacancies.

In the third section we treat the Jahn-Teller effect and Coulomb repulsion, showing how the coupling of the vibronic modes to the electronic states alters the energies of various charge states of the vacancy. The results are still qualitatively similar to the ideal vacancy.

Finally we treat ideal vacancies near the surface. We calculate the vacancy energies as functions of the distance from the vacancy to the surface. The Jahn-Teller effect and Coulomb repulsion are

again ignored because surface vacancies could induce large lattice distortions which are beyond our present understanding. But the qualitative features of ideal vacancies are still interesting.

In the final section, we discuss the possible relationship between vacancies and Schottky barriers in III-V and II-VI semiconductors. We conclude that if vacancies were present in sufficient concentration at the surface of a semiconductor, the band bending would be fixed to a large degree by the defect levels.

II. IDEAL BULK VACANCIES

In this section we present a calculation of the bound state energies and wave functions for ideal vacancies in the bulk of GaSb, GaAs, GaP, InAs, AlAs, InP, ZnTe, CdTe, and ZnSe. The calculations were performed using the Koster-Slater ^(3,4) approach in the tight-binding approximation. "Ideal" vacancy here refers to having ignored lattice relaxation and the Coulombic repulsion among bound electrons, which will be treated in the next section.

In the Koster-Slater approach, the energy and wave function of a bound defect state can be determined by solving ^(3,4)

$$(1 - G_+(\epsilon) V_d)\xi = 0 \quad (4.1)$$

where $G_+(\epsilon)$ is the Green's function at energy ϵ for the perfect crystal, V_d is the defect potential, and ξ is the bound state wave function. We use as a basis one s and three p states on each atom. In our case, the ideal vacancy potential is defined by raising to infinity the on-site energies of the atom to be removed. This prescription is equivalent to setting to zero all the interaction matrix elements involving the removed atom. For the ideal case, the condition for a bound state then becomes ⁽⁵⁾

$$\det |g_+(\epsilon)| = 0 \quad (4.2)$$

where $g_+(\epsilon)$ is the block of $G_+(\epsilon)$ confined to a vacancy site in the tight-binding representation, and so is a 4x4 matrix without spin and an 8x8 matrix with spin. This can be obtained from Eq. (2.5) by setting $\underline{v} = \lambda \underline{1}$ and taking $\lambda \rightarrow \infty$.

The matrix $g_+(\epsilon)$ in (4.2) gives not only the energies of bound states but also their symmetry. Neglecting spin-orbit splitting, $g_+(\epsilon)$ is diagonal in the s-p atomic basis. Six of the diagonal elements (those for p states with spin) are degenerate, and the remaining two (for s states) are also degenerate, so (4.2) reduces to

$$g_{ss}(\epsilon) = 0 \quad \text{or} \quad g_{xx}(\epsilon) = 0 \quad ,$$

where x refers to a p-state oriented along the x-axis. In the first case the state has a_1 (scalar or s-like) symmetry while the second case has t_2 (vector or p-like) symmetry. Spin-orbit splitting breaks the t_2 state into a two-fold and a four-fold state. This splitting is small (<0.1 eV) for vacancy states in the materials considered here (except ZnTe). For simplicity, this splitting will not be explicitly carried through the following discussion, although extension is straightforward and has been done.

The wave function can be recovered, as in Eq. (2.10), once condition (4.2) is satisfied and is (in normalized form)

$$\xi_{\beta}(\vec{r}) = \sum_{\tau j \alpha} \frac{G_{\tau j \alpha, \text{oo}\beta}(\epsilon_{\beta})}{\tau j \alpha [-G'_{\text{oo}\beta, \text{oo}\beta}(\epsilon_{\beta})]^{1/2}} \phi_{j \alpha}(\vec{r} - \vec{R}_{\tau} - \vec{\rho}_j) \quad (4.3)$$

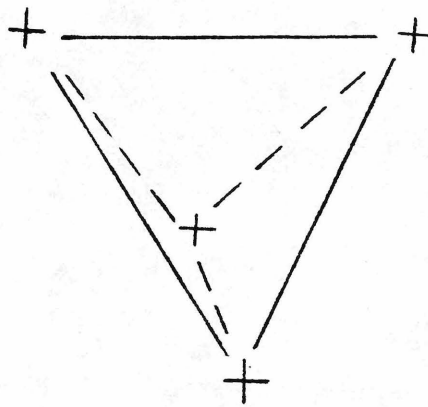
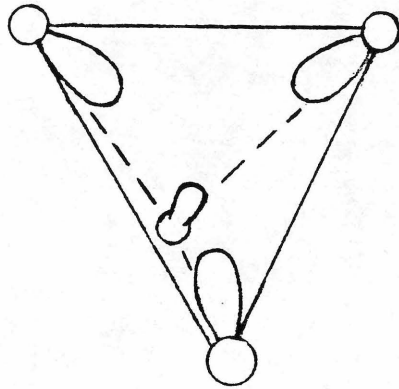
with $\phi_{j\alpha}$ the α -th state on atom j , \vec{R}_τ is the vector to the unit cell τ , and $G_{\tau j\alpha, \beta 00}(\epsilon) = (\phi_{j\alpha}(\vec{r} - \vec{R}_\tau - \vec{\rho}_j) | G_+(\epsilon) | \phi_{0\beta}(\vec{r} - \vec{\rho}_0))$. The prime denotes differentiation with respect to ϵ . The ξ_β has the symmetry of the state β as mentioned above. The vacancy is at site 0.

For each vacancy, then, we expect an a_1 level and a t_2 level as in Fig. 4.1. Viewing the vacancy state as a tetrahedral arrangement of nearest neighbors with dangling sp^3 bonds directed toward the vacancy, one can see that there are four symmetrized arrangements of amplitudes for the dangling bonds. The a_1 state corresponds to the symmetric combination, while the t_2 state has an orbital degeneracy of three and corresponds to the three ways of assigning two positive and two negative amplitudes to the dangling bonds.

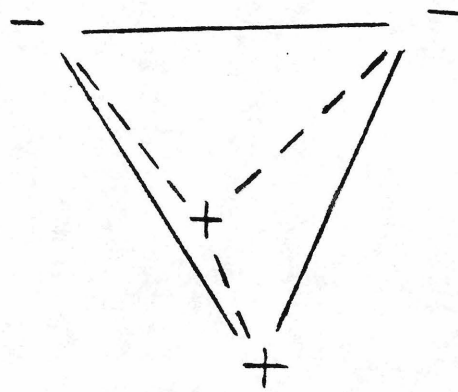
Our results for bulk ideal vacancies in GaSb, GaAs, GaP, InAs, AlAs, and InP are presented in Table 4.1. Each vacancy produces an a_1 and a t_2 level, the latter of which may be slightly split (< 0.1 eV) by spin-orbit interactions. Some levels are resonant in a band. The daggers indicate the highest occupied level in the neutral vacancy.

The positions of the levels can be understood in qualitative terms. In covalent materials, such as GaSb, the valence band is composed of bonding states between neighbors, while the conduction band is anti-bonding. Severing a bond, as creating a vacancy does, produces

Figure 4.1. Schematic of the ideal vacancy configuration in a zinc-blende crystal. The removal of an atom leaves four nearest neighbors in a tetrahedron with their dangling bonds pointing inward. The interaction of these bonds causes a splitting between symmetric (a_1) and tetragonal (t_2) amplitudes.



a_1



t_2

Figure 4.1

Table 4.1. Ideal bulk vacancy levels for GaSb, GaAs, GaP, InAs, AlAs, InP, ZnTe, CdTe, and ZnSe. Below each material is noted the band gap and the ionicity defined in the text. Anion and cation levels are measured relative to the valence band maximum. Daggers indicate the highest occupied level in the neutral vacancy. Asterisks denote where spin-orbit interactions were included.

TABLE 4.1. IDEAL VACANCY LEVELS

Material (Band gap (eV), Ionicity (eV))	Cation Vacancy Levels (eV above VBM)		Anion Vacancy Levels (eV above VBM)	
	a_1	t_2	a_1	t_2
GaSb (0.9, -3.8)	<0	0, 19, 0, 14 ⁺	0, 05	>E _g ⁺
GaAs (1.5, -3.6)	<0	0, 45 ⁺	0, 05	1, 05 ⁺
GaP (2.2, -2.9)	<0	0, 4 ⁺	0, 5	1, 4 ⁺
InAs (0.4, -2.6)	<0	0, 25 ⁺	0, 05	>E _g ⁺
AlAs (2.3, -2.2)	<0	0, 8 ⁺	0, 8	1, 6 ⁺
InP (1.5, -1.9)	<0	0, 45 ⁺	0, 75	>E _g ⁺
ZnTe (1.5, 0.3)	<0	1, 1 ⁺	1, 45 ⁺	>E _g
CdTe (1.6, 1.0)	<0	0, 22, 0, 25 ⁺	>E _g	>E _g
ZnSe (2.8, 1.2)	<0	0, 4, 0, 57 ⁺	2, 5 ⁺	>E _g

a dangling bond which would reasonably have an energy somewhere in between bonding and anti-bonding states, that is, in the gap. In an ionic material like CdTe, the mixing between bonds is lessened, with the valence band becoming more anionic and the conduction band more cationic. An anion vacancy, with cation dangling bonds, should then produce states resonant with the conduction band. Similarly, a cation vacancy should produce states in or near the valence band.

In representing each material by a parameterized Hamiltonian, we include parameters that correspond roughly to free atomic energy levels. Our parameters are constrained to have values for these parameters in agreement with the energy levels from atomic calculations. We then define χ , the ionicity measure, to be the difference between the cation s-state energy and the anion p-state energy. GaAs has $\chi = -3.6$, while CdTe has $\chi = 1.0$, GaAs being more covalent. The materials in Table 4.1 are ordered according to their ionicities.

The vacancy levels do show the trend with ionicity suggested by the previous qualitative argument. This is shown in Fig. 4.2 by GaAs, InP, and CdTe. Anion levels tend to move toward the conduction band with increasingly ionic materials, while cation levels go in the reverse.

Vacancy states in bulk GaAs have been calculated by others using similar and more sophisticated techniques. The main difference between our calculations and other tight-binding work is in the

Figure 4.2. Ideal vacancy levels in GaAs, InP, and CdTe. Cation and anion vacancy levels are shown relative to valence band (VB) and conduction band (CB) for each material. The figure is arranged to demonstrate the trend from covalent to more ionic materials.

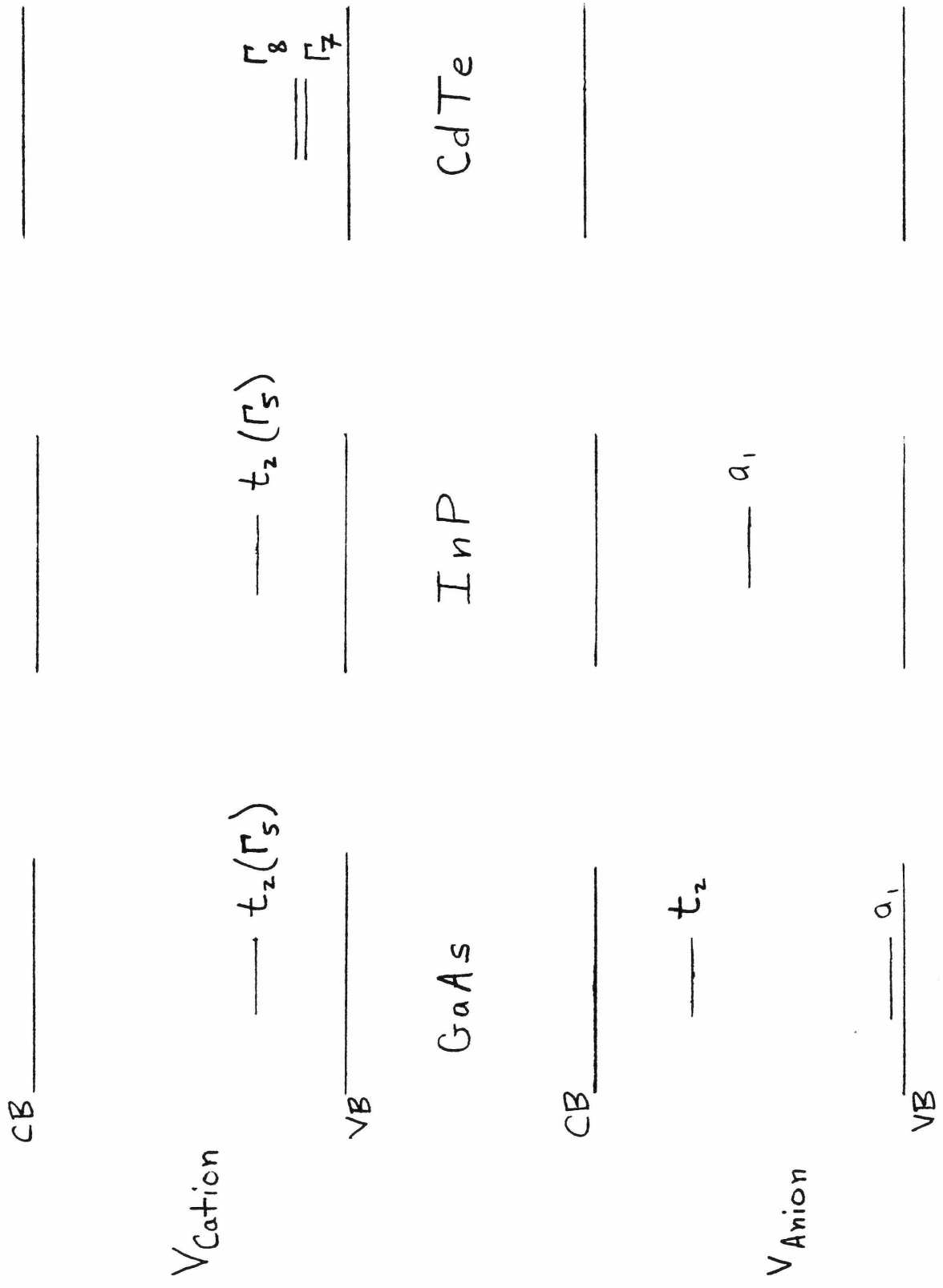


Figure 4.2

parameters used to describe the Hamiltonian ⁽⁵⁾.

Pseudopotential calculations have also been reported for vacancies in bulk GaAs and perhaps represent more accurate results. Jaros and Brand ⁽⁶⁾ use a Green's function approach, like ours, but with a one-electron pseudopotential formalism. They find that an As vacancy has an a_1 level just below the valence band maximum and a t_2 level about 0.4 eV above the conduction band edge, while a Ga vacancy has an a_1 level just below and a t_2 level at about 0.15 eV above the valence band edge. Bachelet, Baraff, and Schlüter, ⁽⁷⁾ using a self-consistent pseudopotential Green's function calculation, find the Ga t_2 level weakly bound about the valence band edge and the As t_2 level at 1.08 eV. The agreement between our results and those of Bachelet, Baraff, and Schlüter is quite good.

So far, no mention has been made of the occupation of the states shown in Fig. (4,2). Neutral anion vacancies in III-V materials have three electrons to put into the defect levels a_1 and t_2 , because, of the eight electrons tied in the four covalent bonds around an As atom, five are removed with the neutral atom. This leaves the six-fold t_2 state with one electron. This degenerate ground state is unstable to lattice distortions, as will be discussed in the next section, but these distortions are ignored in this section. Similarly a neutral cation vacancy in a III-V semiconductor has five electrons, an anion

vacancy in a II-VI semiconductor has two, and a cation vacancy in a II-VI compound has six.

In the approximation of an ideal vacancy, the one-electron energies give the changes in total energy as one changes the occupation of the states. A neutral vacancy in a III-V compound, for example, has an odd number of electrons, so the highest state is only partially occupied. In the ideal approximation, the energy required to remove the highest electron is the same as that gained by putting on a second electron. A neutral vacancy in a II-VI material has an even number of electrons. In the ideal approximation, adding two electrons gives twice as much energy as one electron. Likewise, removing two electrons takes twice as much energy as one.

Because of this ideal approximation, a III-V material with only ideal anion or cation vacancies present, the Fermi level at absolute zero would be at the t_2 energy calculated in this section. For ideal cation vacancies in an otherwise pure II-VI semiconductor, the highest occupied level is 6-fold degenerate and has 4 electrons in it. The Fermi level at absolute zero would again be at the t_2 energy. For ideal anion vacancies in the otherwise pure II-VI semiconductor, the highest occupied level is 2-fold degenerate and is filled. The Fermi level at absolute zero then lies halfway between this level and the lowest unoccupied level.

Impurities in the crystal will cause a charging of the vacancies. If one assumes that the doping concentration is much larger than the vacancy concentration, then the Fermi level in the material is determined by the doping. If the Fermi level lies above the calculated one-electron levels, these levels will be filled. If the Fermi level lies below, the levels will be empty. Hence, the doping determines the charge state of the vacancies.

The ideal approximation is clearly incomplete. One must include the Coulombic repulsion among electrons bound to the defect. This raises the total energy. The lattice around the vacancy will distort, the extent of which is determined by the number of bound electrons. This lowers the total energy. The two effects tend to cancel and do not alter greatly the conclusions of the one-electron calculations. These corrections are included in the next section.

III. CHARGED VACANCY STATES AND THE JAHN-TELLER EFFECT

It was noted in the previous section that ideal vacancies can become charged when doping is added. Clearly two important effects have been neglected. First, we have neglected Coulombic repulsions among localized electrons. The tight-binding parameters we have may, in some lumped and disguised form, reflect Coulombic interactions among Bloch waves, but now we must account for the additional interactions among the electrons localized at the defect. From Eq. (4.3), we calculate that up to 80% of the wave function for the vacancy states is localized on the nearest neighbors of the vacancy, so Coulomb repulsion is not negligible. Second, the lattice relaxation around the vacancy was ignored previously. The void left by the vacancy could certainly allow some modifications in the lattice structure near the defect lowering the total energy. The relaxation depends on the charge state of the vacancy. This latter point, the Jahn-Teller effect ⁽²⁾, represents a breakdown in the Born-Oppenheimer approximation, where now changes in the electronic state can modify strongly the lattice arrangement. These two effects, Coulombic repulsion and lattice distortion, tend to cancel out, but the difference can play an important role in the behavior of the vacancies.

In the absence of an atom, the neighboring lattice will clearly relax. The strength and type of distortion may depend on the electronic configuration, in which case the Born-Oppenheimer approximation breaks down. This occurs when the electronic state is orbitally degenerate ⁽²⁾. This can be seen from

$$(\psi | \frac{\partial H}{\partial Q_i} | \psi) = V_i \quad , \quad (4.4)$$

Here ψ is the ground state electronic wave function calculated for a Hamiltonian $H(\{R\})$, a function of the nuclear positions $\{R\}$, and Q_i is the coordinate of some normal mode displacement of the nuclei. Suppose the group of symmetry operations of H is formed. If ψ transforms like the identity representation of that group, then V_i vanishes for all modes except those not changing the symmetry of H , such as a breathing mode. However, if ψ transforms as some representation other than the identity, V_i might not vanish for symmetry-breaking modes. Thus, orbital degeneracies may be removed by coupling to lattice distortions.

For the case of a vacancy in a zinc blende crystal, the undistorted levels have a_1 and t_2 symmetry. The a_1 level is the identity representation and its two-fold spin degeneracy cannot be removed by lattice distortions. The six-fold t_2 level, on the other hand, is susceptible to splitting by the Jahn-Teller effect when occupied.

Three of the normal modes for vacancies in zinc blende crystals are illustrated in Fig. (4.3). The breather mode does not change the tetrahedral symmetry. The symmetry group remains T_d , and the a_1 and t_2 levels shift without splitting. The tetragonal mode changes the symmetry group from T_d to D_{2d} , splitting the t_2 level into the four-fold e and two-fold b_2 levels. A trigonal distortion has the symmetry group C_{3v} . This mode splits the t_2 level into the two-fold a_1 and four-fold e levels. Other modes exist, but the three discussed here are of most interest in the following.

The electronic states of relaxed neutral vacancies in the bulk of III-V and II-VI semiconductors are illustrated schematically in Fig. (4.4). The number of electrons on the neutral vacancy increases as one goes counterclockwise in the figure starting with the anion vacancy in a II-VI semiconductor, which has two electrons. For the state with two electrons, the a_1 state is filled and only breathing mode distortions can occur. For three electrons, as the anion vacancy in III-V's has, the t_2 level is split by the occupation with one electron. The cation vacancy in III-V's has five electrons, and this splits the t_2 level completely into three two-fold levels. The neutral cation vacancy in a II-VI semiconductor has six electrons, so that the t_2 level is split into four-fold and two-fold levels, with the former being lower and filled,

Figure 4.3. Three lattice distortions for vacancies in zincblende crystals. The breather, tetragonal, and trigonal modes are illustrated, along with the consequences for the a_1 and t_2 levels.

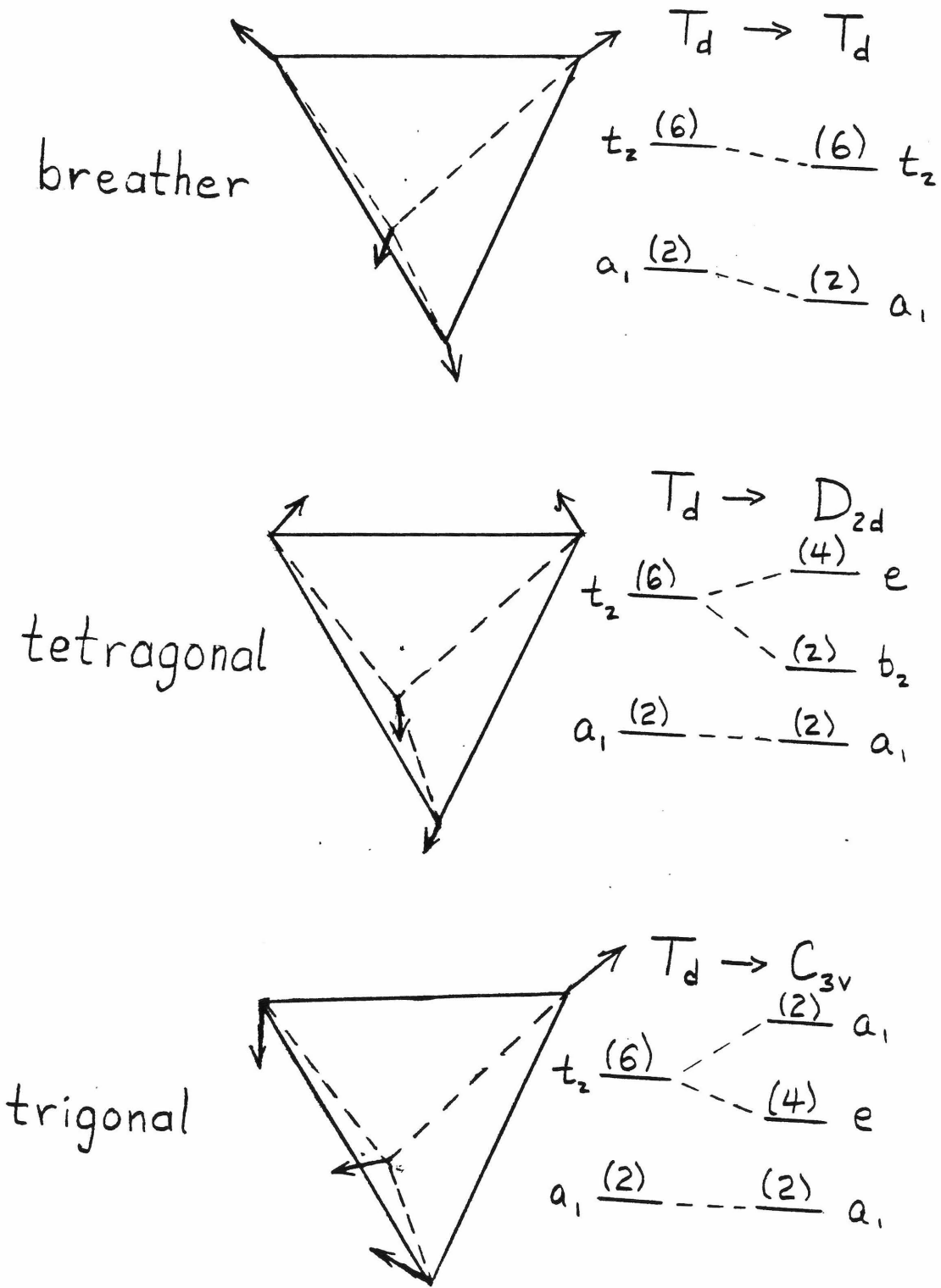


Figure 4.3

Figure 4.4. The electronic states of neutral vacancies in the bulk of III-V and II-VI semiconductors. This schematic picture shows electron occupation (arrows), level splittings a residual degeneracies (arrows).

Neutral Vacancy States
in
III-V's & II-VI's

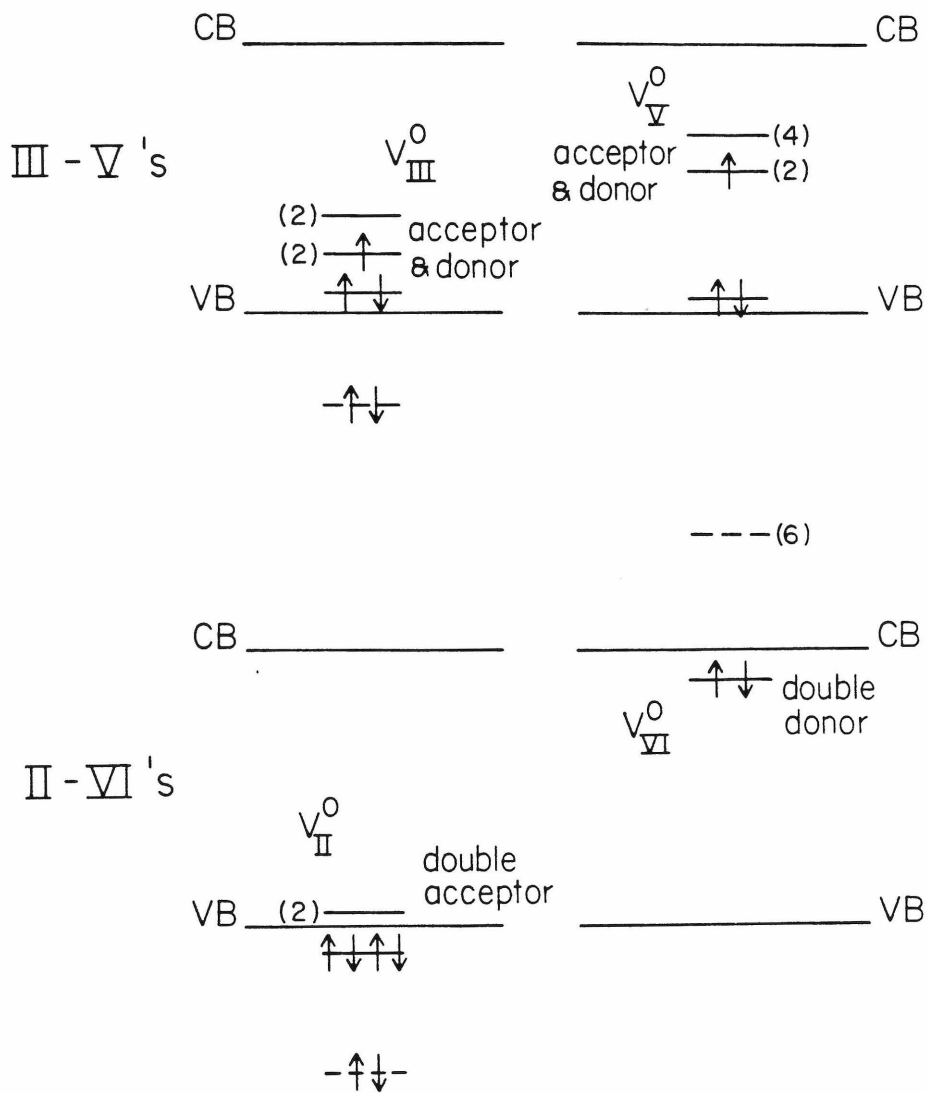


Figure 4.4

We now look in detail at an example of charging. The anion vacancy in a III-V semiconductor can have three charge states: V^+ , V^0 , and V^- . The V^+ has two electrons, both in the a_1 level. The absence of electrons in the t_2 level makes possible only breathing mode distortions which lower the a_1 level. The V^0 has a filled a_1 level and one electron in the t_2 level. In Si, the vacancy with three electrons undergoes a tetragonal Jahn-Teller distortion ^(8,9) We assume that the same holds for the anion vacancy in III-V's. The tetragonal mode splits the t_2 level, allowing the total energy to be lowered. The distortion is such that the two-fold level is lower. The V^- has two electrons in a_1 and two in t_2 . This enhances the tetragonal distortion. We also must account for the Coulomb repulsion between the two electrons bound to the t_2 level. (It is assumed that, as in GaAs, the a_1 level occurs near the valence band and so the electrons in that state are not well localized and do not contribute significantly to additional Coulomb repulsions.)

If we expand the total energies to second order in the tetragonal mode coordinate and take the V^+ state with no distortion as the zero of energy, we have

$$E_+ = \frac{1}{2}kQ^2$$

$$E_0 = \frac{1}{2}kQ^2 + \epsilon - VQ$$

$$E_- = \frac{1}{2}kQ^2 + 2\varepsilon - 2VQ + U \quad , \quad (4.5)$$

Here Q is the displacement of a single atom in the tetragonal distortion, k is the lattice restoring force constant for the displacement, ε is the one-electron energy of the t_2 state of the neutral vacancy with no distortion, V is the Jahn-Teller coupling for this distortion, and U is the electrostatic repulsion for the negatively charged vacancy. The value of Q is fixed by minimizing the energy of each state and so depends on the charge:

$$V^+ : \quad Q = 0$$

$$V^0 : \quad Q = V/k \quad (4.6)$$

$$V^- : \quad Q = 2V/k \quad .$$

The minimum values for the energy are

$$E_+ = 0$$

$$E_0 = \varepsilon - V^2/2k \quad (4.7)$$

$$E_- = 2\varepsilon - 2V^2/k + U \quad .$$

For fixed number of electrons, then, the energy is given by the foregoing. However, the usual circumstance is to have the Fermi level fixed. In that case, the probability of finding the vacancy in

a given charge state V^i is given by

$$P(V^i) = \frac{e^{-(E_i - N_i \mu)/kT}}{\sum_i e^{-(E_i - N_i \mu)/kT}} \quad (4.8)$$

where μ is the chemical potential and N_i is the number of electrons in the t_2 level. At $T = 0$, the lowest of $(E_i - N_i \mu)$ will be occupied, so the charge state depends on μ . Normally, one might expect that as μ is raised, the vacancy goes through the sequence V^+ , V^0 , V^- . The transition between V^+ and V^0 occurs at $\mu(+ \rightarrow 0) = \epsilon - V^2/2k$, and between V^0 and V^- at $\mu(0 \rightarrow -) = \epsilon + U - 3V^2/2k$. However, if $U < V^2/k$, there is no value of μ for which the V^0 state is stable, as pointed out by Baraff, Kane, and Schlüter ⁽¹⁰⁾. This situation is often called an "Anderson negative-U" case ⁽²²⁾. In this case, the transition between V^+ and V^- occurs at $\mu(+ \rightarrow -) = \epsilon - V^2/k + U/2$.

In the top panel of Fig. (4.5), we show the splitting of the charge states of the anion vacancy in a III-V semiconductor for the case of a stable V^0 state.

We estimate the Jahn-Teller coupling V and the Coulomb repulsion U in the bulk using perturbation theory. The unperturbed wave function wave function, ξ_β , is given by Eq. (4.3), where β indicates a t_2 symmetry state. The Jahn-Teller coupling is calculated from

$$VQ = \langle \xi_\beta | \frac{\partial H}{\partial Q} | \xi_\beta \rangle$$

Figure 4.5. The effect of Coulomb repulsion and lattice distortion on the transition energies for the anion vacancy in a III-V semiconductor and a cation vacancy in a II-VI semiconductor. On the left in each case is the two-fold level which is the lowest unoccupied state in the neutral vacancy. The anion vacancy in the III-V compound can gain or lose an electron, while a cation vacancy in the II-VI can gain one or two electrons. The transition energies (Fermi level at which the charge changes) is indicated on the right. Coulomb interactions and Jahn-Teller effects split the various charge states.

Vacancy Charge States

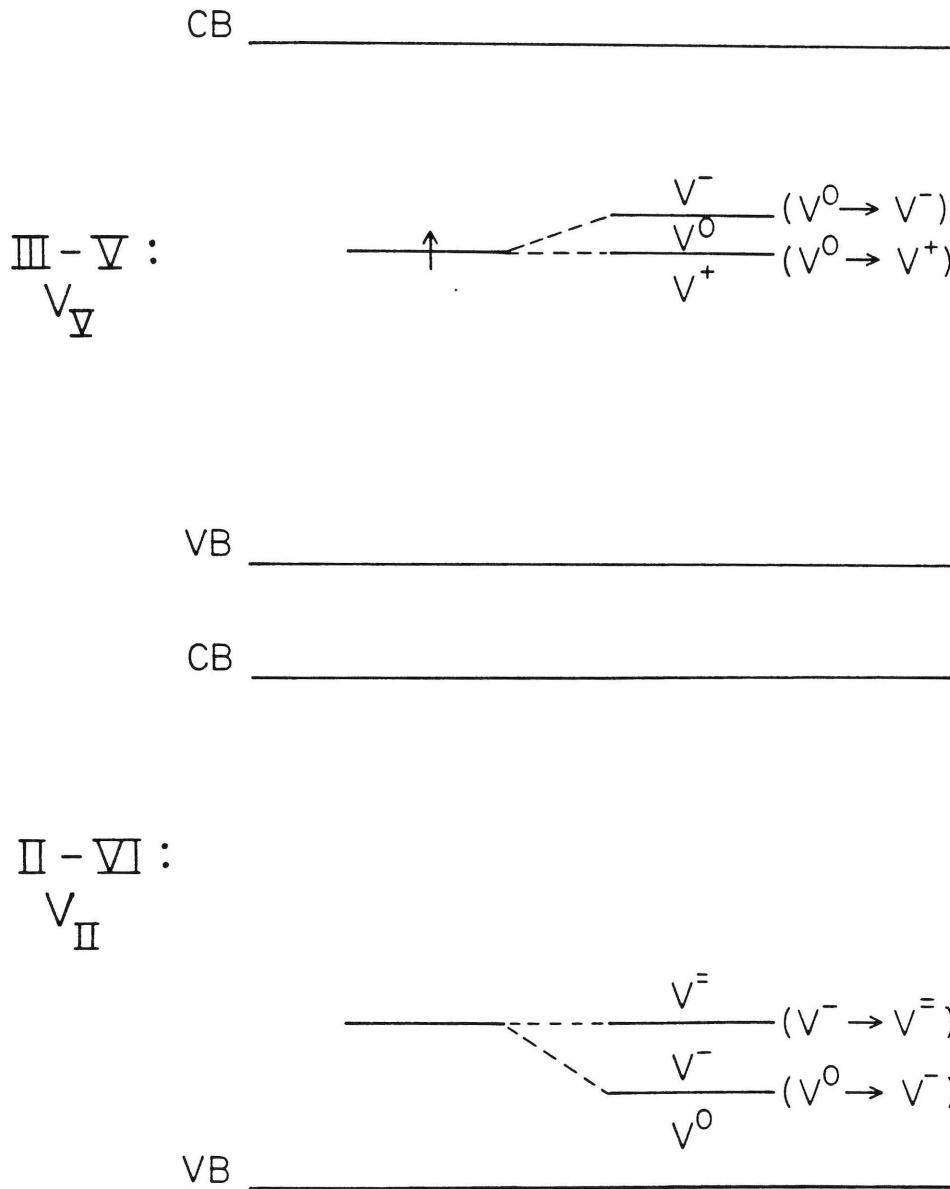


Figure 4.5

where Q is the tetragonal mode displacement. The distortion potential, $\partial H/\partial Q$, is found by assuming that the tight-binding parameters scale like the overlap of the atomic functions ⁽²⁸⁾. For GaAs and AlAs, the tetragonal distortion couplings for the b_2 state are 1.3 eV/\AA^0 and 0.7 eV/\AA^0 , respectively. The e states shift in the opposite direction by half those amounts. The Coulombic repulsion was estimated as

$$U = \langle \xi_\beta(r_1) \xi_\beta(r_2) | \frac{e^2}{\epsilon(r_{12}) |r_{12}|} | \xi_\beta(r_1) \xi_\beta(r_2) \rangle$$

where $[e^2/\epsilon(r) r]$ is the Fourier transform of $(4\pi e^2/\epsilon(q) q^2)$ and $\epsilon(q)$ is the dielectric function ⁽¹¹⁾. One center integrals on the first and second atomic shells were included in the estimate of U . The results were 0.20 and 0.27 eV for GaAs and AlAs, respectively. The force constant k , was estimated by scaling the Keating model calculations of Ref. (10) for Si by the bond stretching force constant determined from compressibility ⁽¹²⁾. The result of this scaling was 12 eV/\AA^2 for both GaAs and AlAs (compared with 14.8 eV/\AA^2 for Si).

These values for the parameters indicate that there is a small stability region for the neutral anion vacancy in GaAs and AlAs, as shown schematically in the top panel of Fig. (4.5). In GaAs, the V^0 is stable for $1.0 \text{ eV} < \mu < 1.05 \text{ eV}$ and in AlAs if $1.6 \text{ eV} < \mu < 1.8 \text{ eV}$. For μ less than the lower bound, V^+ is stable, while for μ higher than the upper bound, V^- is stable.

The cation vacancies in II-VI semiconductors have six electrons in the neutral state. In ZnSe and CdS, the negative cation vacancy is known to have trigonal symmetry ^(8,9) We assume that the distortion for the neutral cation vacancy in the II-VI semiconductors is also trigonal. This splits the t_2 level to two-fold and four-fold levels. The four-fold level goes down and is fully occupied. Thus there is a separation between occupied and unoccupied levels. We will concentrate here on the states formed by adding electrons to the unoccupied, two-fold level: V^0 , V^- , $V^{=}$.

Now the situation is somewhat reversed from that of the anion vacancy in III-V's. There the distortion increases with increasing number of electrons. Here the distortion decreases with added electrons. The reason can be seen as follows. The trigonal distortion splits the t_2 level into two-fold a_1 and four-fold e levels, with the four-fold level lower in energy as in Fig. (4.3). In the V^0 case, this four-fold level is occupied. Adding an electron to the upper a_1 level to make V^- causes the distortion to decrease, lowering the a_1 . In $V^{=}$, there is no distortion because the six-fold t_2 state is non-degenerate when filled.

The energies of the V^0 , V^- , $V^{=}$ states can be written in terms of the trigonal distortion, taking the neutral state with no distortion to be the zero:

$$\begin{aligned}
 E_0 &= \frac{1}{2} kQ^2 - 2VQ + 4(V^2/2k) \\
 E_- &= \frac{1}{2} kQ^2 - VQ + \epsilon + 4(V^2/2k) \\
 E_{\pm} &= \frac{1}{2} kQ^2 + 2\epsilon + U + 4(V^2/2k)
 \end{aligned}
 \tag{4.9}$$

where the symbols are the same as for Equation (4,5), but apply to the trigonal mode. The minimum values for the energy are:

$$\begin{aligned}
 E_0 &= 0 \\
 E_- &= 3(V^2/2k) + \epsilon \\
 E_{\pm} &= 2\epsilon + U + 4(V^2/2k)
 \end{aligned}
 \tag{4.10}$$

If $U > V^2/k$, then the transition between V^0 and V^- occurs for the Fermi level at $\mu(0 \rightarrow -) = \epsilon + 3(V^2/2k)$ and from V^- to V^{\pm} when $\mu(- \rightarrow \pm) = \epsilon + U + V^2/2k$. If $U < V^2/k$, then there is no μ for which the V^- state is stable. The transitions from V^0 to V^{\pm} occurs when $\mu(0 \rightarrow \pm) = \epsilon + U/2 + V^2/k$.

The bottom panel of Fig. (4.5) shows the splitting of the V^0 , V^- , and V^{\pm} levels for a cation vacancy in a II-VI semiconductor, for the case of stable V^- state.

Estimating the parameters V , k and U as before ⁽³⁰⁾ gives for CdTe, $V = 0.4 \text{ eV/\AA}$, $k = 6 \text{ eV/\AA}^2$, and $U = 0.20 \text{ eV}$, and for ZnTe, $V = 0.4 \text{ eV/\AA}$, $k = 8.2 \text{ eV/\AA}^2$, and $U = 0.20 \text{ eV}$. These values indicate that

V^- occurs if $0.3 V < \mu < 0.45$. In ZnTe, the V^- is stable for $1.1 \text{ eV} < \mu < 1.3 \text{ eV}$.

Cation vacancies in III-V semiconductors have five electrons in the neutral state, so that in the ideal case the t_2 level has three electrons in it, and this is unstable to a Jahn-Teller distortion. We have not carried out the analysis for these vacancies. This case is similar to the anion vacancy in III-V's in having an odd number of electrons in the neutral vacancy.

Anion vacancies in II-VI compounds are not affected by symmetry-breaking lattice distortions. These vacancies have two electrons in the neutral state and are susceptible to breathing mode distortions. We have not calculated the breathing mode distortion energy for this case.

IV. IDEAL VACANCIES NEAR THE SURFACE

In this section we present a calculation of bound state energy levels of ideal vacancies near or on a semiconductor surface. We consider the (110) surface of GaSb, GaAs, GaP, InAs, AlAs, InP, ZnTe and CdTe. Effects due to lattice relaxation are ignored in this section.

The calculations were performed in the manner used for ideal bulk vacancies, except that now we describe the surface by using a nine layer slab of atoms. The slab is thick enough to isolate the opposite surfaces from each other and to give less than 0.1 eV deviation from bulk vacancy energies for a vacancy in the center of the slab, this thickness being nine atomic layers.

The equation for a bound state energy is still (4.2), but $g(\epsilon)$ is no longer diagonal owing to the presence of the surface. Near the surface, the bulk symmetry is broken and the a_1 and t_2 states mix to form orbitally nondegenerate levels, three of which have positive parity and one of which has negative parity under the mirror symmetry of the (110) surface.

The results of our calculation for the bound state energies of ideal vacancies near the GaAs (110) surface are shown in Fig. (4.6). A Ga vacancy on the fifth layer from the surface induces an essentially triply degenerate bound state (without spin) 0.4 eV above the valence

Figure 4.6. Energies, relative to the band edges, of ideal vacancies near the (110) surface of GaAs. The bound-state energies are essentially the same as those for bulk until the vacancy reaches the second atomic layer from the surface. The arrow indicates the highest energy state occupied in the neutral vacancy.

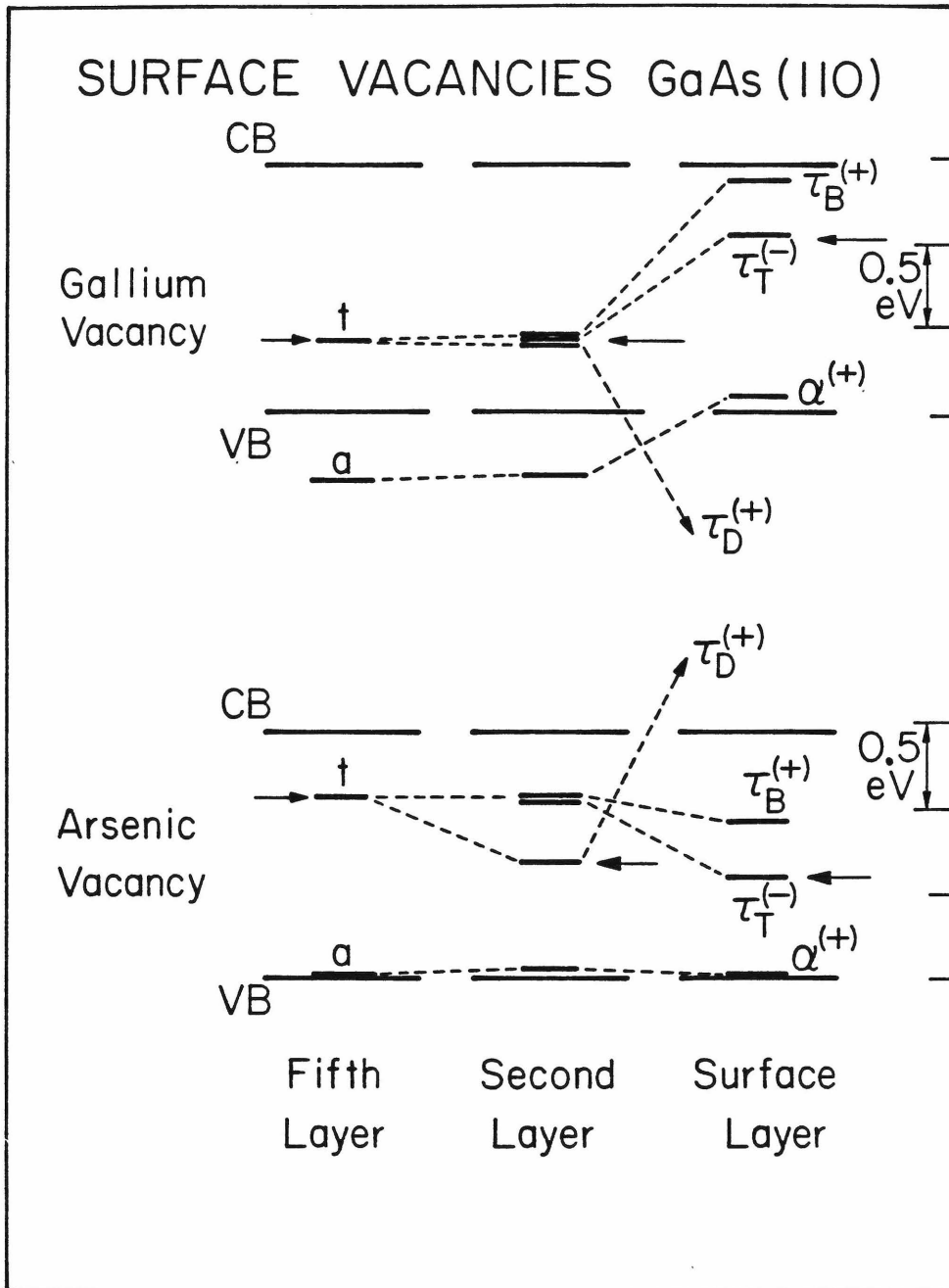


Figure 4.6

band maximum. There is also a well-defined singlet resonance 0.4 eV below the valence band edge. An As vacancy on the fifth layer induces an essentially triply degenerate bound state 1.1 eV above the valence band edge and a singlet level at the valence band edge. The energy positions of the bound vacancy levels on the fifth layer of the slab are essentially the same (to better than 0.1 eV) as those for the bulk.

As a vacancy is moved near the surface, the bound state energy levels are not much changed (by less than 0.1 eV) until the vacancy is put on the second layer from the surface. From an atom on the third atomic layer from the (110) surface, the closest atom absent because of the surface is a fifth nearest neighbor (and only 1 of 12 fifth nearest neighbors is absent). For an atom on the second atomic plane, a second nearest neighbor is removed because of the surface and the degenerate triplet levels are split by an appreciable amount. Arrows indicate the highest occupied level in the neutral vacancies. The highest occupied level of the Ga vacancy moves to higher energy as the vacancy is moved toward the surface, while the highest occupied level of the As vacancy moves to lower energy. The direction of motion near the surface can be understood in terms of the bonds near the surface. Because of relaxation, the hybridization of the surface cation orbitals involved in the bonding is sp^2 rather than sp^3 as in the bulk. As a result, an anion vacancy on the second atomic layer breaks one sp^2 bond and this is

of lower energy than the bulk sp^3 bonds because of its larger s character. For an anion vacancy on the surface layer, two sp^2 bonds are broken and again the bound states are at lower energy than the bulk. The surface anion orbitals involved in the bonding have become trigonal as a result of the relaxation, and so have larger p character. Therefore, second or surface layer cation vacancies, in having these trigonal bonds around them, are at higher energy than the bulk cation vacancies.

The labeling of the states in Fig. (4.6) is based on the character of the wave functions of the states. We examined the unitary transformation $u(\epsilon)$ which diagonalizes the Green's function $g(\epsilon)$ and determines the orbital decomposition of the atomic functions on the vacancy site which generates the bound state (in the sense of Eq. (4.2)). In the bulk, this decomposition consists of the s state and the 3 p states which generate the a_1 and t_2 levels, respectively. Near the surface the decomposition is mixed and depends both on the position and type of vacancy. However, the states labeled $\alpha^{(+)}$ are generated largely by the s level. The states labeled $\tau_T^{(-)}$ are generated by the p orbital which lies in the plane of the surface and changes sign under the mirror symmetry of the (110) surface. The states labeled $\tau_B^{(+)}$ are generated largely by the p orbital which lies in the plane of the surface and is even under the mirror symmetry. The states labeled $\tau_D^{(+)}$ are generated

largely by the p orbital which is orthogonal to the surface (i.e., the surface dangling bond state).

In Fig. (4.7) we show similar results for vacancies near the (110) surface of InP, arranged to show comparison to GaAs. We noted in the first section that as one went from covalent to more ionic materials, anion vacancy levels tended to move to higher energy. At the same time cation vacancy levels tend to lower energy (see Fig. (4.2)). The same trends hold for vacancies near the surface: The more ionic InP shows almost uniform upward shift of anion vacancy levels for all depths from the surface relative to GaAs, and small downward shift for the cation vacancy levels. The trend with ionicity is preserved for vacancies near the surface.

In Fig. (4.8) we show results for vacancies near the (110) surface of two II-VI compounds; CdTe and ZnTe. Cation vacancies produce levels in the gap, similar in nature to those in III-V's. Anion vacancies produce deep states in ZnTe but not in CdTe. The relationship between vacancy states in ZnTe and CdTe can be understood again by noting that CdTe is more ionic than ZnTe.

Figures 4.7a and 4.7b. Energy levels, relative to the band edges, of ideal vacancies near the (110) surface of InP and GaAs. Cation vacancy levels are shown in (4.7a), and anion levels in (4.7b). The bound state levels are essentially the same as those in bulk until the vacancy reaches the second atomic layer from the surface. The arrows indicate the highest state occupied in the neutral vacancy.

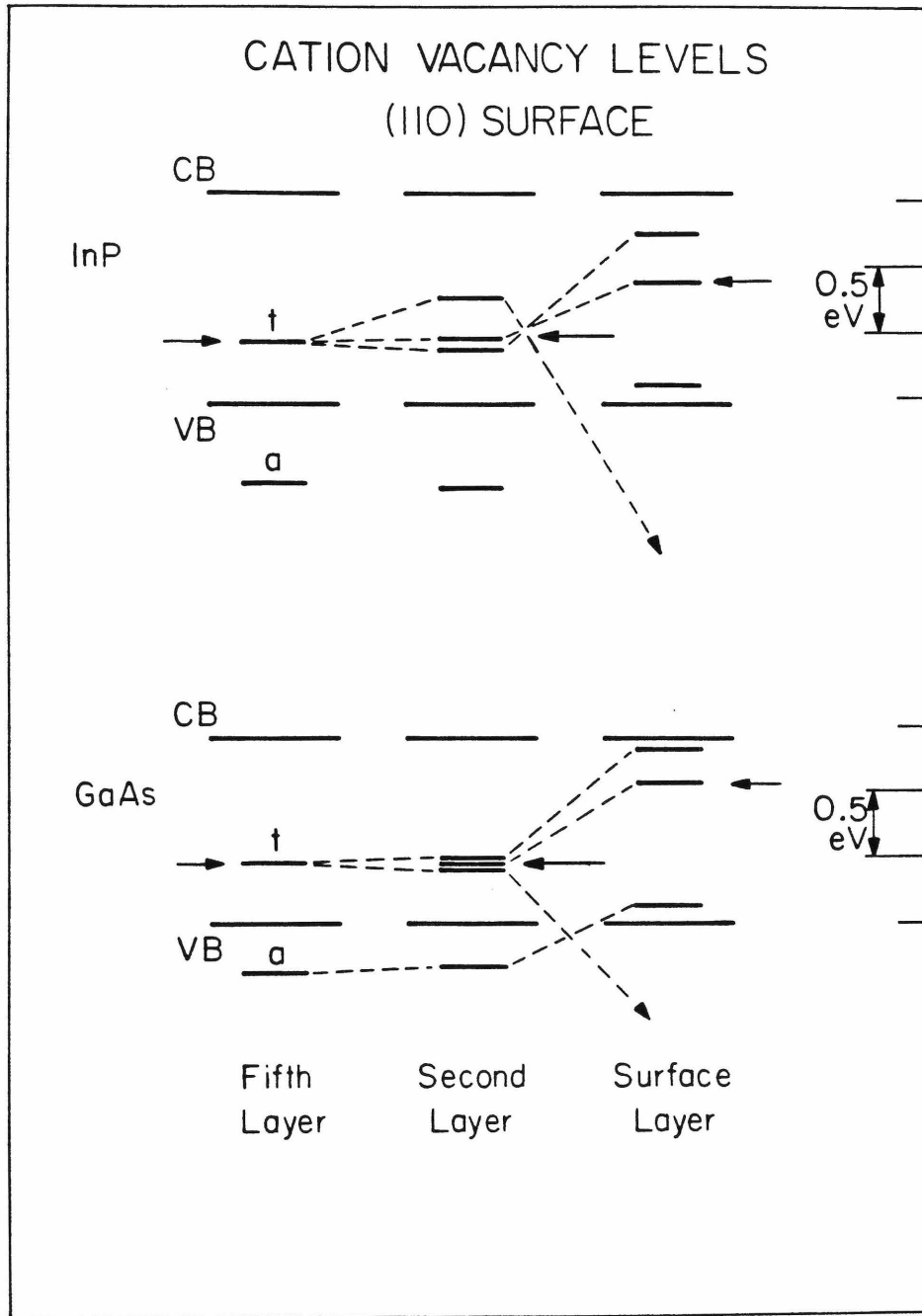


Figure 4.7a

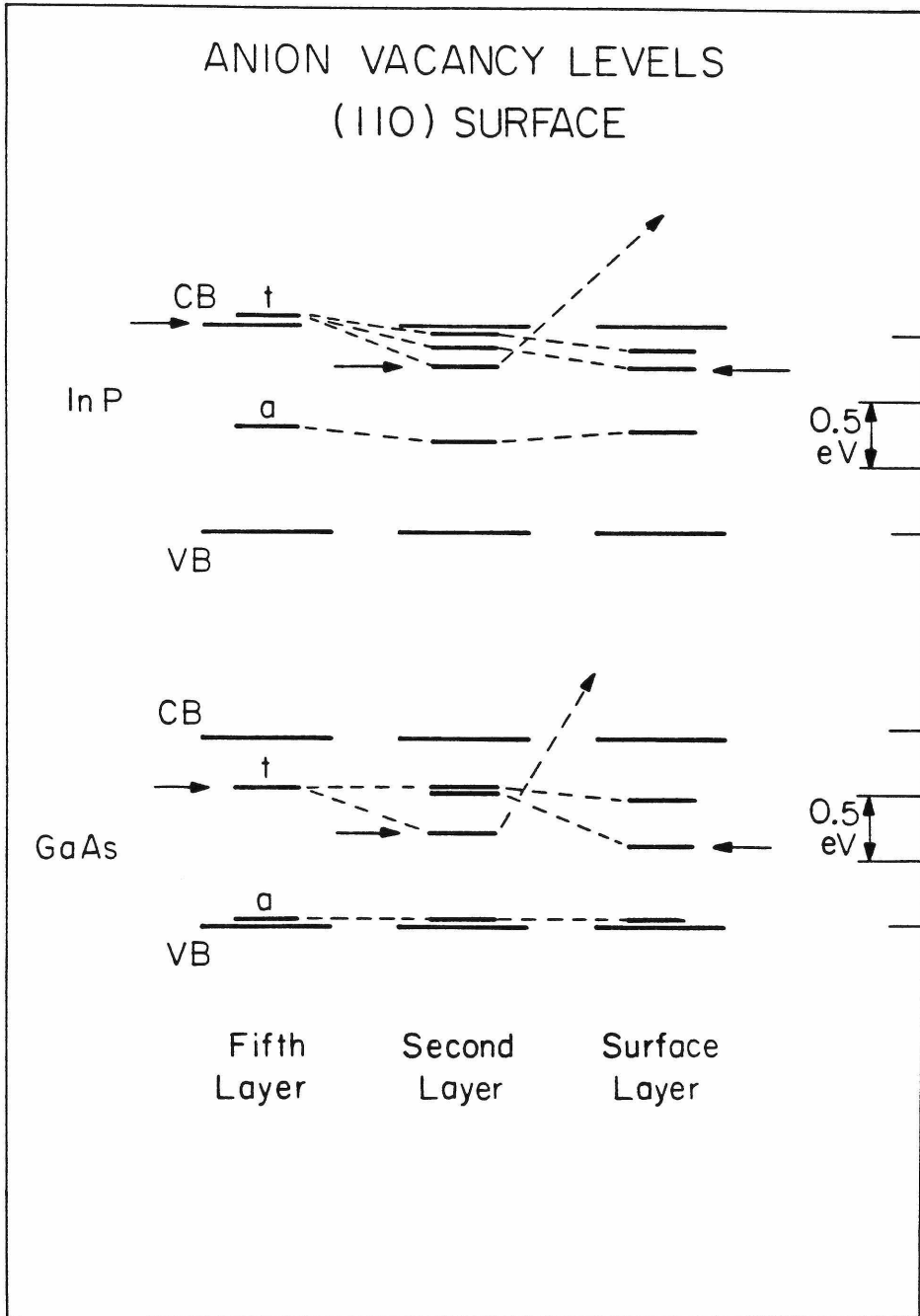


Figure 4.7b

Figure 4.8. Energy levels, relative to the band edges, of ideal cation vacancies near the (110) surface of CdTe and ZnTe. The bound state levels are essentially the same as those in bulk until the vacancy reaches the second atomic layer from the surface. The arrows indicate the highest occupied state in the neutral vacancy.

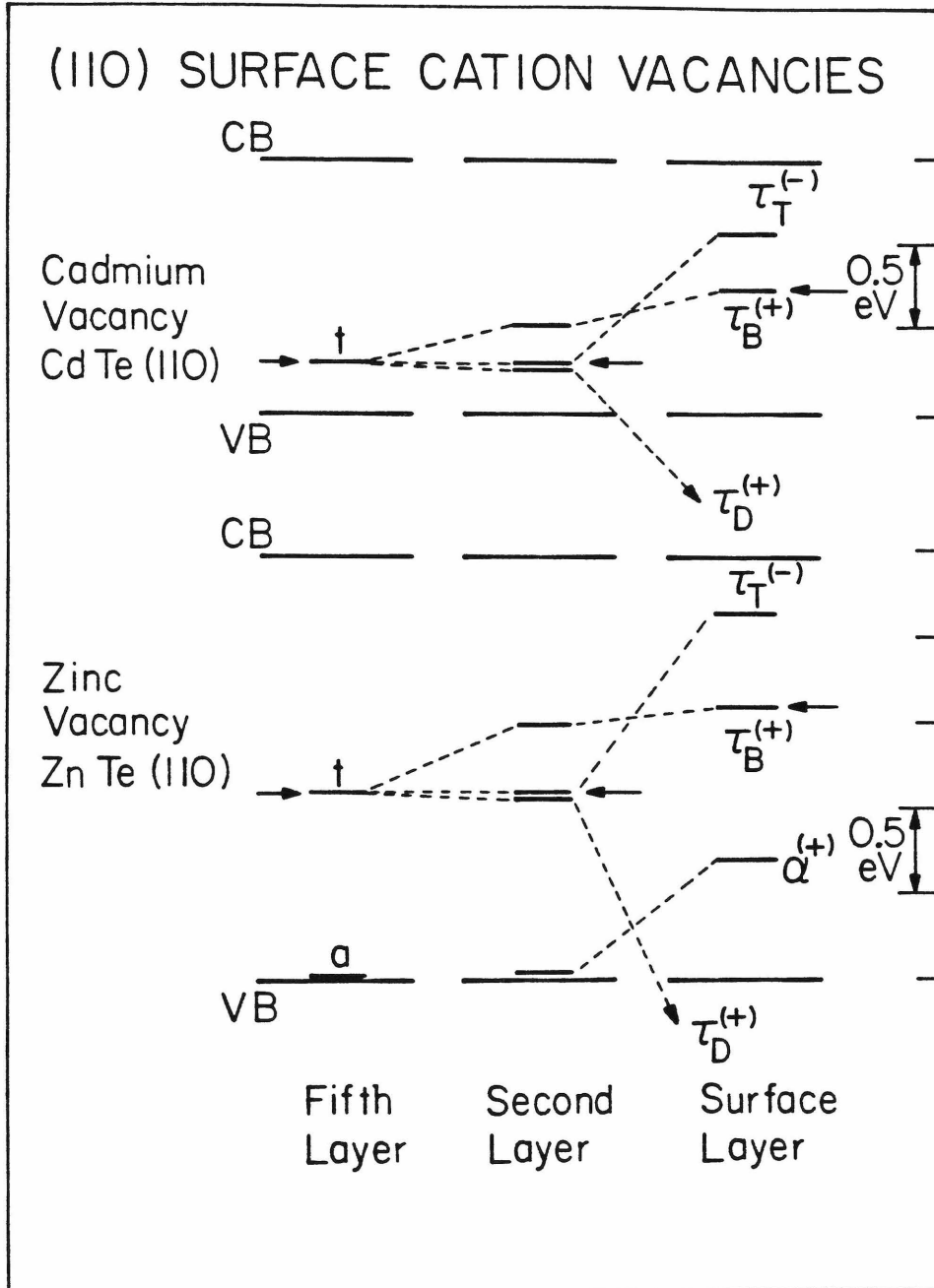


Figure 4.8

V. VACANCIES AND SCHOTTKY BARRIERS

There has emerged recently a new model of Schottky barrier formation in III-V's: the Defect Model ⁽¹³⁾. Two observations led to this proposal ⁽¹⁴⁾. The first was that clean, well-cleaved semiconductor surfaces had no band bending, and that the bands bent when slight contamination was present. The second was that the band bending reached an asymptotic value rather independent of adatom, reminiscent of the metal-independent band bending of fully-formed Schottky barriers.

The Defect Model seems to explain naturally the foregoing observations. The energy liberated by adsorption of metal or oxygen may produce defects that would not be present on a perfect surface. These defects could cause levels deep in the band gap that in turn could pin the Fermi level. The pinning position would then be independent of the adatom,

There are three other criteria for which any explanation of the band bending in III-V's must account. In the case of the free surface with some contamination, the asymptotic values of the Fermi level relative to the surface bands are different for n- and p-type semiconductors ^(13,14). The difference is about 0.3 eV for many adatoms on (110) GaAs. Also, the Fermi level pinning seems to move toward the conduction band as one considers increasingly ionic materials.

In addition, the Schottky barrier appears to obey a common anion rule in the III-V's (except those involving Al), and some II-VI's (15). That is, for two materials with the same anion, the barrier for holes appears to be the same. Compounds containing Al violate this rule.

Spicer and co-workers^(13,14) proposed a dual defect model, two defects associated with missing cations and anions. The defect caused by missing anions would pin the n-type and that associated with missing cations the p-type. There is some evidence against this suggestion (16).

An alternative, the Single Defect Model presented here, is that anion vacancies in III-V semiconductors can account for all the observed behavior. Vacancies in III-V's can charge with either sign, and so pin both n- and p-type materials.

It seems very unlikely that only one type of defect is present or is active in causing the pinning. But calculations of a large variety of defect states at this time seem pointless. However, certain qualitative behavior can be expected from classes of defects, and this can be explored by calculating simple cases, such as vacancy levels.

In II-VI semiconductors, the situation is unclear. No clear UPS data are available for a II-VI semiconductor as they are for III-V's. The Schottky barrier data are also inconclusive for II-VI's. Since these inadequacies are generally due to the natural

instabilities of the compounds which may be compensated for in the future, it seems worthwhile to explore the vacancy states in these materials.

To judge the Single Defect Model of Schottky barrier formation, we therefore examine our calculated levels in III-V's and II-VI's in light of the criteria outlined above. In particular, we calculate the pinning positions for n- and p-type materials given a sufficient density of vacancies, compute vacancy levels in semiconductors with different ionicities to compare with the ionicity trend, and also calculate levels in semiconductors with the same anion to check with the common anion rule.

We considered in Section III the energies of charged vacancy states for vacancies in III-V's and II-VI's. The charge state of the vacancy depends on the Fermi level. In the bulk, one would assume that usually the vacancy concentration is small compared to that of impurities. In that case, the chemical potential is fixed by the shallow dopants and that fixes the charge state of the vacancies as discussed in Section III. However, in the Defect Model for Schottky barrier formation, it is assumed that there is a large concentration of defects in a thin layer near the semiconductor surface. In this case, the position of the band edges at the surface relative to the Fermi level will be determined by the defects. For the case of a free surface (without a macroscopic metal overlayer), the defects near the surface will charge

so as to compensate the charge in the depletion region of the semiconductor.

Let us consider vacancies near the surface of a III-V semiconductor. In this case the charge of the vacancies can be positive, negative or neutral. From electrostatics, the Fermi level measured relative to the valence band maximum at the surface, μ_s , in n-type material is given by

$$\mu_s = \mu - \frac{2\pi e^2}{\epsilon_0} \frac{(N_+ - N_-)^2}{n_d} \quad (4.11)$$

where

$$(N_+ - N_-) = N_V [P(V^+) - P(V^-)] \quad (4.12)$$

Here n_d is the donor concentration, ϵ_0 is the semiconductor dielectric constant and N_+ , N_- and N_V are the number per unit area of positively charged, negatively charged and all vacancies, respectively. $P(V^i)$ is the probability that the charge state V^i will exist, as in Eq. (4.8) with μ replaced by μ_s . In p-type material, n_d in Eq. (4.11) is replaced with $(-n_a)$.

For a Schottky barrier with a macroscopic metal overlayer on a III-V semiconductor, the defects charge and form a dipole with their image charge in the metal. The charge state of the defects

need not be opposite to that in the space charge region because the metal overlayer can screen the space charge. Taking the vacancies to lie in a plane a distance ℓ from the metal surface, μ_s in n-type material is given by

$$\mu_s = (I_s - \chi_m) + D_I + \frac{4\pi e^2 \ell}{\epsilon_d} \left\{ (N_+ - N_-) + n_d x_d \right\} \quad (4.13)$$

Here I_s is the semiconductor ionization potential, χ_m is the metal work function, x_d is the depletion length, D_I is any additional (perhaps chemically induced) dipole layer which may occur at the interface and ϵ_d is the dielectric constant of the disordered region at the interface. In p-type material n_d in Eq. (4.13) is replaced with $(-n_a)$.

At room temperature, kT is very small compared to the energy scale of interest. Thus, the function $(N_+ - N_-)$ will change very rapidly as μ_s moves past the stability points for the vacancy charge states. As a result, for a sufficiently high surface density of vacancies, μ_s will be pinned at one of the stability points. In Table (4.2), we list the stability points at which the pinning occurs and the minimum surface density of vacancies required to pin for the various possibilities. From this table, we see that the vacancy charge state, and hence the relevant stability point at the free surface, depends on the semiconductor doping. However, in the Schottky barrier case, the vacancy charge state and relevant

TABLE 4.1. Surface Fermi level and surface vacancy concentration to complete pinning for various conditions.

	V ⁰ Stable		V ⁰ Unstable	
	Schottky Barrier	Free Surface	Schottky Barrier	Free Surface
V ⁻	$\mu_s = \epsilon - \frac{3V^2}{2k} + U$ $N_V \geq \frac{\mu_s - (I_s - \chi_m + D_I)}{4\pi e^2 \ell / \epsilon_d}$ $\mu_s \geq I_s - \chi_m + D_I$	$\mu_s = \epsilon - \frac{3V^2}{2k} + U$ $N_V \geq \left[\frac{n_d \epsilon_0 (\mu - \mu_s)}{2\pi e^2} \right]^{1/2}$ <p>n-type</p>	$\mu_s = \epsilon - \frac{V^2}{k} + \frac{U}{2}$ $N_V \geq \frac{\mu_s - I_s - \chi_m - D_I}{4\pi e^2 \ell / \epsilon_d}$ $\mu_s > I_s - \chi_m + D_I$	$\mu_s = \epsilon - \frac{V^2}{k} + \frac{U}{2}$ $N_V \geq \left[\frac{n_d \epsilon_0 (\mu - \mu_s)}{2\pi e^2} \right]^{1/2}$ <p>n-type</p>
V ⁰	$\mu_s = I_s - \chi_m + D_I$ $N_V \geq 0$ $\epsilon - \frac{V^2}{2k} \leq \mu_s \leq \epsilon - \frac{3V^2}{2k} + U$	$\mu_s = \mu$ $N_V \geq 0$ $\epsilon - \frac{V^2}{2k} \leq \mu_s \leq \epsilon - \frac{3V^2}{2k} + U$	<p>---</p>	<p>---</p>
V ⁺	$\mu_s = \epsilon - \frac{V^2}{2k}$ $N_V \geq \frac{I_s - \chi_m + D_I - \mu_s}{4\pi e^2 \ell / \epsilon_d}$ $\mu_s \leq I_s - \chi_m + D_I$	$\mu_s = \epsilon - \frac{V^2}{2k}$ $N_V \geq \left[\frac{n_d \epsilon_0 (\mu_s - \mu)}{2\pi e^2} \right]^{1/2}$ <p>p-type</p>	$\mu_s = \epsilon - \frac{V^2}{k} + \frac{U}{2}$ $N_V \geq \frac{I_s - \chi_m + D_I - \mu_s}{4\pi e^2 \ell / \epsilon_d}$ $\mu_s < I_s - \chi_m + D_I$	$\mu_s = \epsilon - \frac{V^2}{k} + \frac{U}{2}$ $N_V \geq \left[\frac{n_d (\mu_s - \mu)}{2\pi e^2} \right]^{1/2}$ <p>p-type</p>

stability point depends on $(I_S - \chi_m + D_I)$. Consequently, it is possible that μ_S may differ for the free surface of an n- and p-type semiconductor, but doping does not significantly influence μ_S in a macroscopic Schottky barrier.

In order that μ_S be approximately equal for metals in which $(I_S - \chi_m + D_I)$ has opposite signs, it is necessary to charge the defect region with opposite polarities. Simple donors and acceptors can charge with only one sign. Thus a single donor or acceptor defect cannot account for the independence of μ_S on χ_m observed in the III-V semiconductors, whereas a level which can charge with either sign (such as the anion vacancy) can account for this observation.

For the case of As vacancies near the free GaAs surface, taking the parameters V , k , and U from our bulk calculations indicates that V^0 is stable, as mentioned in Section III. In this case the n-type and p-type materials should be pinned about 0.1 eV apart, in rough agreement with the 0.3 eV difference reported by Spicer, et al.^(13,14). Thus the n- and p-type pinning difference can be accounted for by this model.

The ionicity trend of Schottky barriers is displayed by Table (4.3). In the series of materials shown, the Fermi level moves from near the valence band maximum to nearer the conduction band. The sequence is arranged by ionicity, going from covalent to more

TABLE 4,3, Comparison of the surface Fermi level relative to valence band maximum (E_F) with the scaled electronegativity parameter for the common III-V semiconductors. The value for E_f from Ref. is for oxidized surfaces; the numbers in parentheses (without parentheses) are for n-type (p-type) material. All numbers are in units of eV.

	χ^a	E_f (Ref.)	E_f (Ref.)	E_g
GaSb	-5.0	0	0.1 (0.1)	0.67
InSb	-4.0	0		0.16
AlSb	-3.5	0.55		1.63
GaAs	-3.5	0.5	0.5 (0.7)	1.43
GaP	-2.7	0.7		2.24
InAs	-2.6	0.5		0.33
AlAs	-2.2	1.1 ^b		2.16
InP	-2.0	0.8	1.1 (1.2)	1.34

a) Ref. ()

b) From the n barrier assuming n and p barriers add to the band gap.

ionic. From Section II, we recall that the same trend is followed by ideal anion vacancies. Cation vacancies generally tend in the opposite direction. Anion vacancies then obey the trend with ionicity.

The common anion rule (15) represents another test that the Single Defect Model passes. To show this, we calculated ideal anion vacancy levels near the surface of alloys such as $\text{Ga}_x\text{Al}_{1-x}\text{As}$ and $\text{Ga}_x\text{In}_{1-x}\text{As}$, as functions of x . The hole barrier in the latter alloy is relatively independent of mole fraction, x , while in the former alloy the hole barrier shows marked dependence.

In Fig. 4.9, we show the calculated energy positions of the highest occupied level in the neutral anion vacancy (the charging level) in the bulk, second atomic layer and first atomic layer from the (110) surface of $\text{Ga}_x\text{In}_{1-x}\text{As}$ and $\text{Ga}_x\text{Al}_{1-x}\text{As}$. Levels in third and deeper layers are close to those for the bulk. The calculated positions of the conduction band minima are also shown. (In the In-rich $\text{Ga}_x\text{In}_{1-x}\text{As}$ alloys, the calculated energy levels move above the conduction band minimum. For these compositions the defect induced levels are resonances rather than bound states. The Fermi level would be fixed by the conduction band minimum rather than by the defect-induced level in these compositions.) The lower panel in Fig. (4,9) shows the measured position of the Fermi level relative to the valence band maximum of the interface for Au Schottky barriers. The measured positions of the conduction band

Figure 4.9. In the upper panels, the calculated positions of the highest occupied state in the neutral anion vacancy as a function of composition in $\text{Ga}_{1-x}\text{In}_x\text{As}$ and $\text{Ga}_x\text{Al}_{1-x}\text{As}$ are shown. Results for vacancies in the bulk, second atomic layer, and on the (110) surface are presented. The energy zero is the valence band maximum; the calculated position of the conduction band minimum is also shown. The lower panels show the measured position of the surface Fermi level as a function of alloy composition in the same materials. The data represented by crosses are from Ref. 22, solid squares from Ref. 23, and inverted triangles from Ref. 18. The conduction band measurements are from Ref. 24.

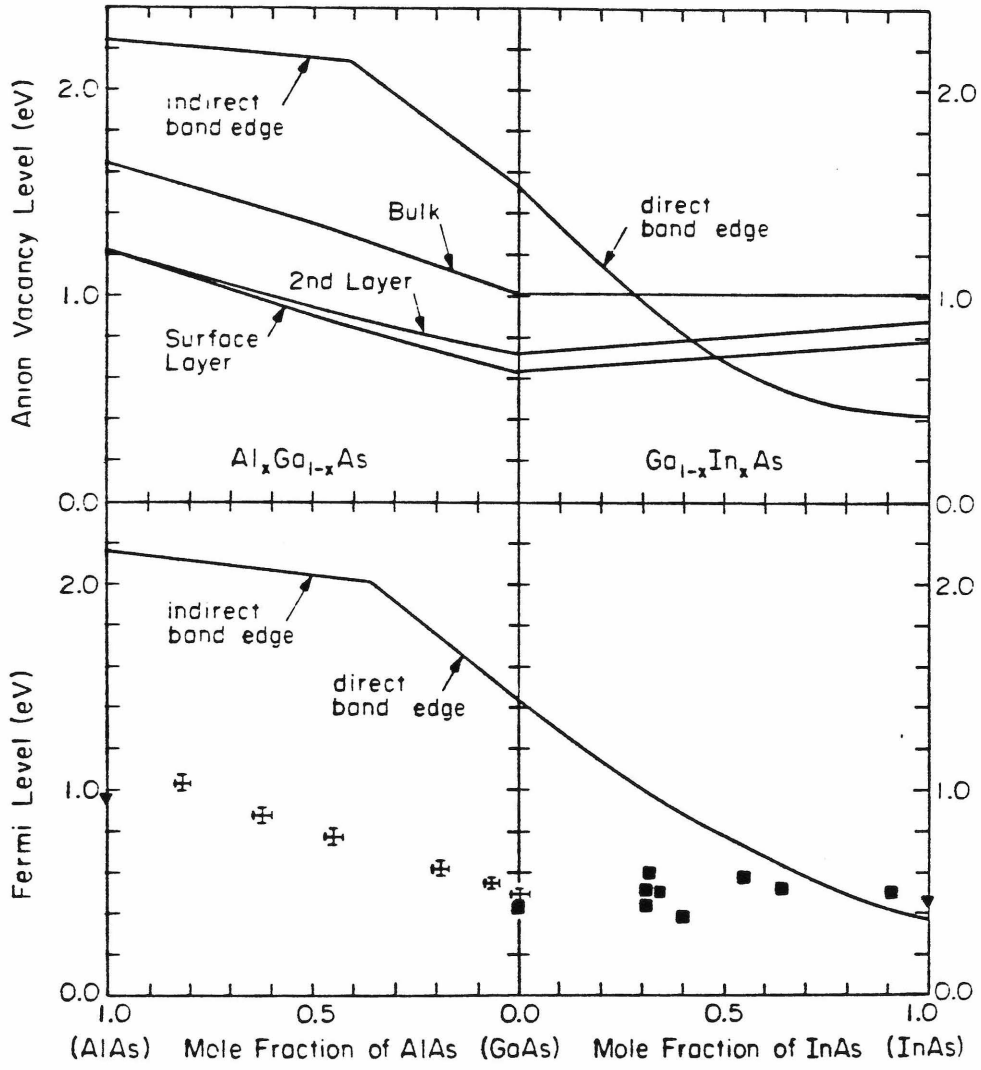


Figure 4.9

minima are also shown. From this figure, we see that the calculated position of the anion vacancy levels are relatively weak functions of composition in the $\text{Ga}_x\text{In}_{1-x}\text{As}$ alloy system. The energy positions, relative to the valence band maximum, increase by less than 0.2 eV as the In mole fraction increases from zero to unity. By contrast, the energy positions of the anion vacancy levels in the alloy $\text{Ga}_x\text{Al}_{1-x}\text{As}$ are much more sensitive functions of composition, increasing by about 0.6 eV as the Al mole fraction increases from zero to unity. Comparing the calculated levels with the measured Fermi level positions, we see a good correlation. There is some uncertainty in the absolute values of the calculated energy levels, but we believe that the trends with composition are significant. The GaInAs system represents a case in which the common anion rule is satisfied and the GaAlAs system represents an exception to this rule.

Figure (4.10) shows the analogous, calculated positions and measurements for $\text{Ga}_x\text{In}_{1-x}\text{P}$. Comparing the calculated anion vacancy levels with the measured Fermi level positions, we again see good correlation as x is varied. The GaInP alloy system satisfies the common anion rule.

In III-V semiconductors, it seems quite plausible that vacancies, particularly anion vacancies, are responsible for Fermi level pinning. A single vacancy can behave as both donor and acceptor. Furthermore,

Figure 4.10. The calculated positions of the highest occupied state in the neutral anion vacancy as a function of alloy composition in $\text{Ga}_{1-x}\text{In}_x\text{P}$ are shown in the upper panel. Results for vacancies in the bulk, second atomic layer, and on the (110) surface are presented. The energy zero is the valence band maximum; the calculated position of the conduction band minimum is also shown. The lower panel shows the measured position of the surface Fermi level as a function of alloy composition in GaInP. Data represented by crossed circles are taken from Ref. ; band edge measurements from Ref. . The solid square is from Ref. .

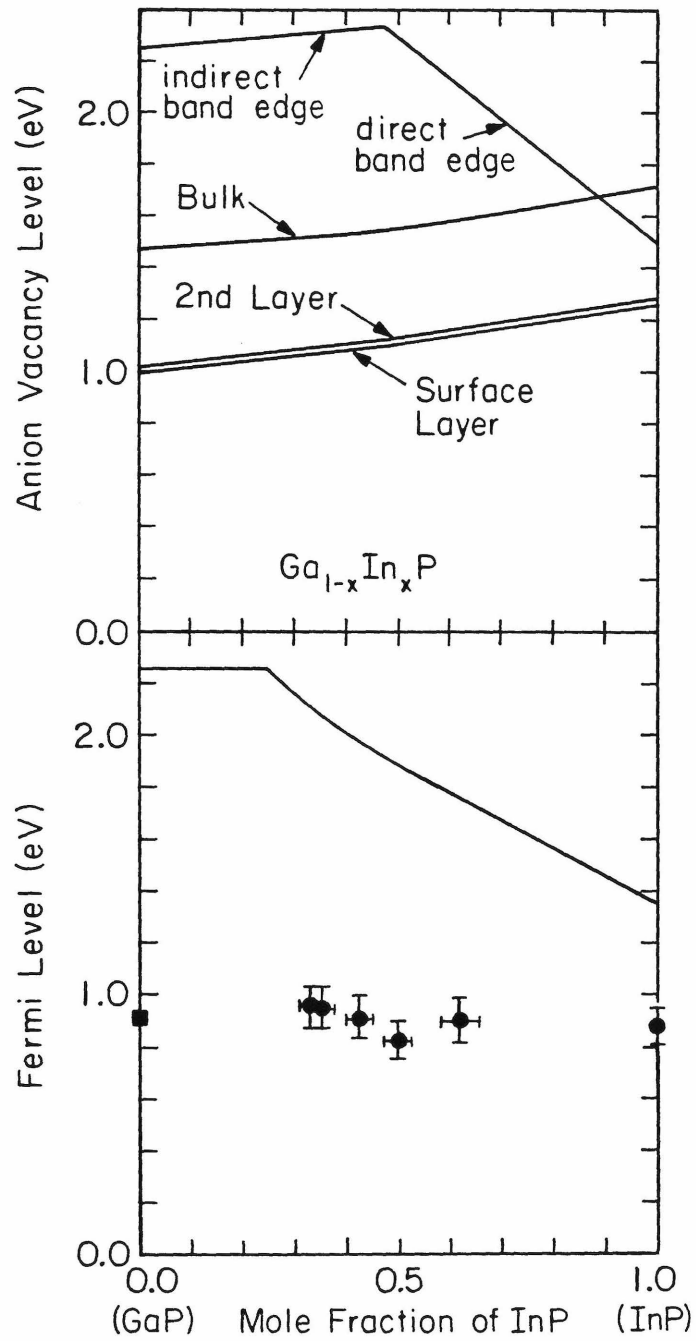


Figure 4,10

the trends in anion vacancy levels with ionicity and with composition of common anion alloys are in agreement with the data.

In II-VI semiconductors, the nature of the vacancy levels is very different (as we saw in Section III). Anion vacancies are double donors. The bulk cation vacancy in CdTe is a double acceptor. In ZnTe, the bulk cation vacancy can act as both donor and acceptor. Near the surface, levels like the donors in CdTe, which are in the valence band in bulk may get pushed up into the gap (see Fig. (4.8)). In general, the Fermi level should be pinned between the highest occupied state and the lowest unoccupied state in the neutral vacancy.

At the present time there are only limited data on the values of the fully formed Schottky barriers on CdTe⁽¹⁸⁾ and ZnTe. These data have been used to argue for a common anion rule for these materials⁽¹⁵⁾. The Schottky barrier on p-type material with Au contacts is approximately the same for CdTe and ZnTe. Comparing these observations with our results, we note that the pinning position for anion vacancies is too close to the conduction band edge. For cation vacancies, we would not predict a common anion behavior. Thus the role of simple vacancies in pinning the Fermi level in II-VI semiconductors is not so clear.

In summary, it seems quite plausible that anion vacancies determine the Fermi level position at III-V surfaces. The

role of cation vacancies in III-V Schottky barriers is unlikely due to their behavior when the ionicity is varied. In II-VI semiconductors, anion vacancies are probably not involved because they induce levels very high in the gap. The role of cation vacancies in determining the Schottky barrier in II-VI's is uncertain.

VI. SUMMARY

In this chapter we calculate the energy levels of vacancies in the bulk and on the (110) surface of nine zinc blende materials. Using the Koster-Slater approach from Chapter 2, the ideal vacancy states in bulk and near the surface are computed. The effects of lattice distortion and Coulomb repulsion are treated perturbatively for bulk vacancies.

Generally it is found that the vacancy levels are dependent on the ionicity of the material. Cation vacancy states move toward the valence band as one considers increasingly ionic materials, while anion states move toward the conduction band. The ideal vacancy levels change by less than 0.1 eV as a vacancy is moved to the surface until it reaches the second atomic layer from the surface. Lattice distortion and Coulomb repulsion in bulk vacancies produce a splitting between the various charge states. These splittings are estimated.

Finally, the possible relationship between vacancies and Schottky barriers is discussed. It is concluded that anion vacancies can account for the observed Fermi level pinning on III-V semiconductors.

APPENDIX

The point group of the zincblende crystal is T_d , which consists of all those operations which send a regular tetrahedron into itself. The subgroups of T_d of interest in this thesis are C_{3v} and D_{2d} , C_{2v} , and C_s . We give here for reference their double group character tables and a compatibility table. The notation is that of Koster, et al ⁽²¹⁾. The basis functions S_x , S_y , and S_z are pseudo-vectors. The functions $\phi(1/2)$ and $\phi(3/2)$ are spinors.

CHARACTER TABLES

T_d	E	E	$8C_3$	$\frac{3C_2}{3C_2}$	$6S_4$	$6\bar{S}_4$	Bases
$a_1(\Gamma_1)$	1	1	1	1	1	1	R or xyz
$a_2(\Gamma_2)$	1	1	1	1	-1	-1	S_x, S_y, S_z
$e(\Gamma_3)$	2	2	-1	2	0	0	$(2z^2 - x^2 - y^2), \sqrt{3}(x^2 - y^2)$
$t_1(\Gamma_4)$	3	3	0	-1	1	1	S_x, S_y, S_z
$t_2(\Gamma_5)$	3	3	0	-1	-1	-1	x, y, z
Γ_6	2	-2	-1	0	$\sqrt{2}$	$-\sqrt{2}$	$\phi(1/2)$
Γ_7	2	-2	-1	0	$-\sqrt{2}$	$\sqrt{2}$	$\Gamma_6 \times \Gamma_2$
Γ_8	4	-4	1	0	0	0	$\phi(3/2)$

D_{2d}	\bar{E}	E	$2S_4$	$2\bar{S}_4$	C_2	$2C_2'$	$2\sigma_d$	Bases
					\bar{C}_2	$2\bar{C}_2'$	$2\bar{\sigma}_d$	
$a_1(\Gamma_1)$	1	1	1	1	1	1	1	R
$a_2(\Gamma_2)$	1	1	1	1	1	-1	-1	S_z
$b_1(\Gamma_3)$	1	1	-1	-1	1	1	-1	$x^2 - y^2$
$b_2(\Gamma_4)$	1	1	-1	-1	1	-1	1	xy or z
$e(\Gamma_5)$	2	2	0	0	-2	0	0	S_x, S_y
Γ_7	2	-2	$\sqrt{2}$	$-\sqrt{2}$	0	0	0	$\phi(1/2)$
Γ_8	2	-2	$-\sqrt{2}$	$\sqrt{2}$	0	0	0	$\Gamma_6 \times \Gamma_3$

C_{3v}	E	E	$2C_3$	$2\bar{C}_3$	$3\sigma_V$	$3\bar{\sigma}_V$	Bases
$a_1(\Gamma_1)$	1	1	1	1	1	1	R or Z
$a_2(\Gamma_2)$	1	1	1	1	-1	-1	S_z
$e(\Gamma_3)$	2	2	-1	-1	0	0	$S_x \pm i S_y$
Γ_4	2	-2	1	-1	0	0	$\phi(1/2)$
Γ_5)	1	-1	-1	1	i	-i	$\phi(3/2, \pm 3/2)$
Γ_6)	1	-1	-1	1	-i	i	

Γ_5 and Γ_6 are degenerate by time-reversal symmetry.

C_{2v}	E	E	$\frac{C_2}{C_2}$	$\frac{\sigma_y}{\sigma_v}$	$\frac{\sigma_{v'}}{\sigma_{v''}}$	Bases
$a_1(\Gamma_1)$	1	1	1	1	1	z
$b_1(\Gamma_2)$	1	1	-1	1	-1	S_y or x
$a_2(\Gamma_3)$	1	1	1	-1	-1	S_z or xy
$b_2(\Gamma_4)$	1	1	-1	-1	1	S_x or y
Γ_5	2	-2	0	0	0	$\phi(1/2)$

C_s	E	E	σ	$\bar{\sigma}$	Bases
$a(\Gamma_1)$	1	1	1	1	S_z or x or y
$b(\Gamma_2)$	1	1	-1	-1	S_x or S_y or z
Γ_3	1	-1	i	-i	} $\phi(1/2)$
Γ_4	1	-1	-i	i	

Γ_3 and Γ_4 are degenerate by time-reversal.

COMPATIBILITY TABLE

T_d	Γ_1	Γ_2	Γ_3	Γ_4	Γ_5	Γ_6	Γ_7	Γ_8
D_{2d}	Γ_1	Γ_2	$\Gamma_1 + \Gamma_3$	$\Gamma_2 + \Gamma_5$	$\Gamma_4 + \Gamma_5$	Γ_6	Γ_7	$\Gamma_6 + \Gamma_7$
C_{3v}	Γ_1	Γ_2	Γ_3	$\Gamma_2 + \Gamma_3$	$\Gamma_1 + \Gamma_3$	Γ_4	Γ_4	$\Gamma_4 + \Gamma_5 + \Gamma_6$
C_{2v}	Γ_1	Γ_3	$\Gamma_1 + \Gamma_3$	$\Gamma_2 + \Gamma_3$ $+ \Gamma_4$	$\Gamma_1 + \Gamma_2$ $+ \Gamma_4$	Γ_5	Γ_5	$2\Gamma_5$
C_s	Γ_1	Γ_2	$\Gamma_1 + \Gamma_2$	$\Gamma_1 + 2\Gamma_2$	$2\Gamma_1 + \Gamma_2$	$\Gamma_3 + \Gamma_4$	$\Gamma_3 + \Gamma_4$	$2\Gamma_3 + 2\Gamma_4$

REFERENCES

1. See the review by S. T. Pantelides, *Rev. Mod. Phys.*, 50, 797 (1978).
2. H. A. Jahn and E. Teller, *Proc. Roy. Soc.*, A161, 220 (1937).
3. G. F. Koster and J. C. Slater, *Phys. Rev.* 95, 1167 and 96, 1208 (1954).
4. J. Callaway, *J. Math. Phys.* 5, 783 (1964), J. Callaway, *Phys. Rev.* 154, 515 (1967).
5. J. Bernholc and S. T. Pantelides, *Phys. Rev.* B18, 1780 (1978).
6. M. Jaros and S. Brand, *Phys. Rev.* B14, 4494 (1976).
7. G. B. Bachelet, G. A. Baraff, M. Schlüter (to be published).
8. G. D. Watkins, in Lattice Defects in Semiconductors-1974, edited by F. A. Huntley, Institute of Physics, Conference Series No. 23 (Institute of Physics, Bristol and London, 1975) p. 1.
9. G. D. Watkins, Proceedings of the 1972 Reading Conference on Radiation Defects in Semiconductors, (Institute of Physics, London, 1973), p. 228.
10. G. A. Baraff, E. O. Kane, and M. Schlüter, *Phys. Rev. Lett.* 43, 956 (1979).
11. J. Bernholc and S. T. Pantelides, *Phys. Rev.* B15, 4935 (1977).
12. J. Waser and L. Pauling, *J. Chem. Phys.* 18, 747 (1950).
13. J. Lindau, P. W. Chye, C. W. Garner, P. Pianetta, C. Y. Su, and W. E. Spicer, *J. Vac. Sci. Technol.* 15, 1332 (1978). P. W. Chye, I. Lindau, P. Pianetta, C. M. Garner, C. Y. Su, and W. E. Spicer, *Phys. Rev.* B18, 5545 (1978).

14. W. E. Spicer, I. Lindau, P. Skeath, and C. Y. Su, *J. Vac. Sci. Technol.* 17, 1019 (1980).
15. J. O. McCaldin, T. C. McGill, and C. A. Mead, *Phys. Rev. Lett.* 36, 56 (1976).
16. R. W. Grant, J. R. Waldrop, S. P. Kowalczyk, and E. A. Kraut, *J. Vac. Sci. Technol.* 16, 1370 (1979).
17. W. E. Spicer, P. W. Chye, P. R. Skeath, C. Y. Su, and I. Lindau, *J. Vac. Sci. Technol.* 16, 1370 (1979).
18. C. A. Mead, *Solid-State Electron.* 9, 1023 (1966).
19. E. J. Mele and J. D. Joannopoulos, *Phys. Rev.* B17, 1528 (1978).
20. J. C. Slater, Quantum Theory of Matter (McGraw-Hill, New York, 1968).
21. C. F. Koster, J. O. Dimmock, R. G. Wheeler, and H. Statz, Properties of the Thirty-two Point Groups (MIT Press, Cambridge Mass. 1963).
22. P. W. Anderson, *Phys. Rev. Lett.* 34, 953 (1975).
23. J. S. Best, *Appl. Phys. Lett.* 34, 522 (1979).
24. K. Kajiyama, Y. Mizushima, and S. Sakata, *Appl. Phys. Lett.* 23, 458 (1973).
25. The CBM's for GaAlAs are from B. Monemar, K. H. Shih, and G. D. Petit, *J. Appl. Phys.* 47, 2604 (1976). Those for GaAuAs are from Ref. 24.
26. T. Kuech and J. O. McCaldin, *J. Vac. Sci. Technol.* 17, 891 (1980).
27. A. Onton, M. R. Lorenz, and W. Renten, *J. Appl. Phys.* 42, 3420 (1971).

28. F. Herman and S. Skillman, Atomic Structure Calculations, (Prentice-Hall, New Jersey, 1963).
29. These calculations neglect the spin-orbit splitting of the states.